Peter Fawdon[1*], M.R. Balme[1], J. M. Davis, J. C. Bridges[3], S. Gupta[4] and C. Quantin-Nataf[5]

[1]The Open University, Walton Hall, Milton Keynes MK7 7EA United Kingdom,
[2]Department of Earth Sciences, Natural History Museum, Cromwell Road, Kensington, London, SW7 5BD, UK,
[3]Space Research Centre, School of Physics and Astronomy, University of Leicester LE1 7RH, UK,
[4]Department of Earth Sciences and Engineering, Imperial College London, London, SW7 2AZ, UK,
[5]Laboratoire de Géologie de Lyon, Université Lyon 1, Bâtiment Géode, 2 Rue Raphael Dubois, 69622 Villeurbanne Cedex, France

Corresponding author: Peter Fawdon (peter.fawdon@open.ac.uk)

Key Points:

- Oxia Planum has a substantial catchment area which experienced at least two phases of fluvial activity from the mid-Noachian to Hesperian
- The fluvial system suggests that Oxia Planum formed in an alluvial or a lacustrine/deltaic environment and later altered by ground water
- Paleolakes in the catchment are likely to have been sustained by ground water but are poorly connected to fluvial system and Oxia Planum

Word count: (main text) 8100

Abstract

Oxia Planum, the landing site for the ExoMars rover mission, is a shallow basin on the southern margin of Chryse Planitia that hosts remnants of sediment fans associated with the ancient channel system Coogoon Vallis. This indicates runoff from a catchment in Arabia Terra has transported material into the landing site. To explore this fluvial system we created a model catchment for Oxia Planum and, using 6 m/pixel ConTeXt camera (CTX) orbital remote sensing image data, we digitised the fluvial and lacustrine landforms in Western Arabia Terra in and around this catchment. We find: (1) The catchment has a minimum area of ~2.1×10^5 km^2 and has been episodically deformed by tectonic activity; (2) There were at least two phases of fluvial activity. The first created a mature landscape associated with Coogoon Vallis, which may have deposited alluvial or deltaic deposits in the Oxia Basin. After a substantial hiatus, a second phase of activity incised u-section channels into the pre-existing landscape and channel systems; and (3) Evidence for numerous possible paleolake deposits within the catchment. These are not well connected to the fluvial system and were probably sustained by ground water activity contemporaneous with both phases of fluvial activity. This groundwater might have modified the

geochemistry of Oxia Planum. Oxia Planum probably experienced an alluvial or distal deltaic/lacustrine depositional environment during the mid Noachian, which was later overprinted by a younger phase of fluvial activity.

Plain language summery

Oxia Planum is the landing site for the ExoMars rover, looking for evidence of ancient life on Mars. The rover will investigate regions where the rocks represent environments most like Earths, and where there is evidence for past liquid water. We explore ancient rivers that drained into Oxia Planum because they could have transported evidence of life into the landing site. The oldest and largest river is Coogoon Vallis. Where this river ended helps us understand the formation of rocks in Oxia Planum. If the river ended where it does today, the rocks may have formed underwater or at a coast line. However, if the river extended further northeast, the rocks may have formed as flood plains. More recently younger rivers brought water through Oxia Planum. These were shorter lived events but the associated groundwater may have altered the chemistry of bedrock in Oxia Planum. We also find that groundwater may have supported lakes in the areas where the rivers came from, but most did not overflow into rivers that lead to Oxia Planum. This means that any ancient life that could have lived in them is less likely to have been transported to the Oxia Planum landing site.

Introduction

Oxia Planum is the landing site for the European Space Agency and Roscomos ExoMars 2022 mission (Vago et al., 2018). The primary goal of the ExoMars *Rosalind Franklin* rover is to search for evidence of ancient life on the surface and subsurface of Mars. The rover will use the *Pasteur* instrument suite to search for physical and chemical biosignatures on samples collected from up to 2 m below the surface (Vago et al., 2017). To meet this ambitious mission goal, it is crucial to understand the geological context of geochemical processes that have occurred in Oxia Planum. In particular, it is important to understand the nature of aqueous activity that has occurred within the landing site because these processes will have had a strong influence on the surface paleoenvironment and the geochemistry of the sub-surface environment, and thus the potential for the preservation, concentration and possible formation of biosignatures.

Oxia Planum (Figure 1) is located at the northern edge of Arabia Terra at ~20°W & 18°N where the ancient cratered terrains transition into the low-lying plains of Chryse Planitia. The landing ellipse for *Rosalind Franklin* is within a small (80 km × 80 km) topographic basin (hereafter referred to as the *Oxia Basin*) within Late Noachian Highlands (Figure 1; lNh; Tanaka et al., 2014). To the south and west of the *Oxia Basin* are extensive clay-bearing units identified in Observatoire pour la Minéralogie, l'Eau, les Glaces et l'Activité (OMEGA; Bibring et al.,

2006) and Compact Reconnaissance Imaging Spectrometer for Mars (CRISM; Murchie et al., 2007) infrared hyperspectral data (Figure 1, Quantin-Nataf et al., 2021). The north of the basin is open to Chryse Planitia, where the clay-bearing terrains are overlain by Chryse Basin fill materials (Greeley et al., 1977; Tanaka, 1997), and toward the southeast margin of the basin are several inlet channels associated with the remnants of several sediment fans (Hynek et al., 2010; Molina et al., 2017; Quantin-Nataf et al., 2021). These sediment fan remnants appear to be associated with Coogoon Vallis and, although the exact relationship is obscured by Kilkhampton crater (IAU, 2019; Figure 1c), the channel systems that enter the *Oxia Basin* from the east, along with a group of unnamed channels from the south, are likely to have supplied water and sediment into the basin from Arabia Terra.

Valley networks on Mars, first observed by Mariner 9 (Masursky, 1973) have long been considered evidence of overland flow and erosion by water in the ancient past (Fassett and Head, 2011; Grant, 2000; Howard et al., 2005; Irwin III and Howard, 2002). As our understanding of the variety of channel forms and their morphology has increased with improvements in data coverage and resolution (Hynek et al., 2010; V. Baker et al., 1983), it is now possible to pick out increasingly subtle channel forms that record surface water action throughout martian history. Recent observations of a regional network of inverted channel-belt depositional systems demonstrate evidence for aggradational river systems in Arabia Terra, and their detailed geomorphology suggests they formed over substantial time periods as a result of regional precipitation (Balme et al., 2020; Davis et al., 2016; Williams et al., 2009). Some of these inverted fluvial systems transition into erosional valley networks south of Arabia Terra, but it remains unclear how these ancient fluvial systems relate to Chryse Planitia, the natural sink for regional fluvial activity, but into which few channels seem to debouch.

The aim of this work is to better constrain the timing of the fluvial activity in the region, and the provenance of sedimentary material that may be present in the landing site. To do this we investigate the morphology and extent of paleo-fluvial landforms associated with Oxia Planum. Using the continuous coverage of ConTeXt camera (CTX; Malin et al., 2007) data to pick out increasingly subtle channel forms, we explore the density and distribution of fluvial geomorphology.

We also use a hydrological model to reveal the catchment of the contemporary *Oxia Basin* and compare it with ancient fluvial activity in the paleo-catchment to estimate the size of the paleo-catchment which drained into the *Oxia Basin* and the *Rosalind Franklin* landing site. We characterise the fluvial and lacustrine landforms observed within the model catchment and determine the relative timing and evolution of aqueous inputs into the *Oxia Basin*. Finally, we consider the evidence for lacustrine activity and consider the implications for biosignature formation, transportation and preservation, the prime targets for the *Rosalind Franklin* rover, from the fluvial history of the catchment.

Figure 1: location and catchment map

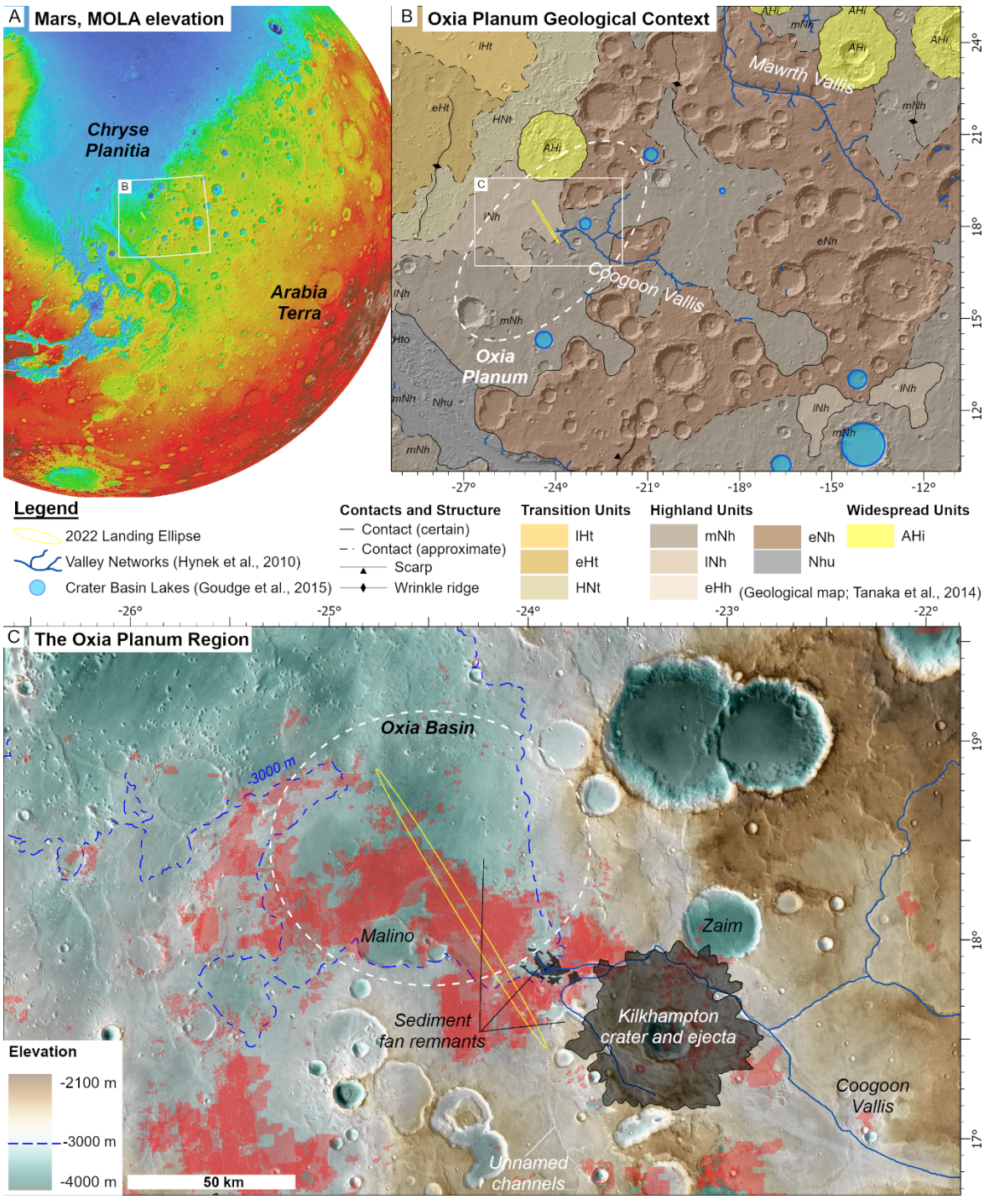
A Mars, MOLA elevation
Chryse Planitia
Arabia Terra
B
B Oxia Planum Geological Context
Mawrth Vallis
Coogoon Vallis
Oxia Planum
C
lHt
eHt
HNt
AHi
mNh
lNh
eNh
Nhu
-27°
-24°
-21°
-18°
-15°
-12°
24°
21°
18°
15°
12°
Legend
2022 Landing Ellipse
Valley Networks (Hynek et al., 2010)
Crater Basin Lakes (Goudge et al., 2015)
Contacts and Structure
Contact (certain)
Contact (approximate)
Scarp
Wrinkle ridge
Transition Units
lHt
eHt
HNt
Highland Units
mNh
lNh
eHh
eNh
Nhu
Widespread Units
AHi
(Geological map; Tanaka et al., 2014)
-26°
-25°
-24°
-23°
-22°
C The Oxia Planum Region
Oxia Basin
3000 m
Malino
Zaim
Sediment fan remnants
Kilkhampton crater and ejecta
Coogoon Vallis
Unnamed channels
Elevation
-2100 m
-3000 m
-4000 m
50 km
19°
18°
17°

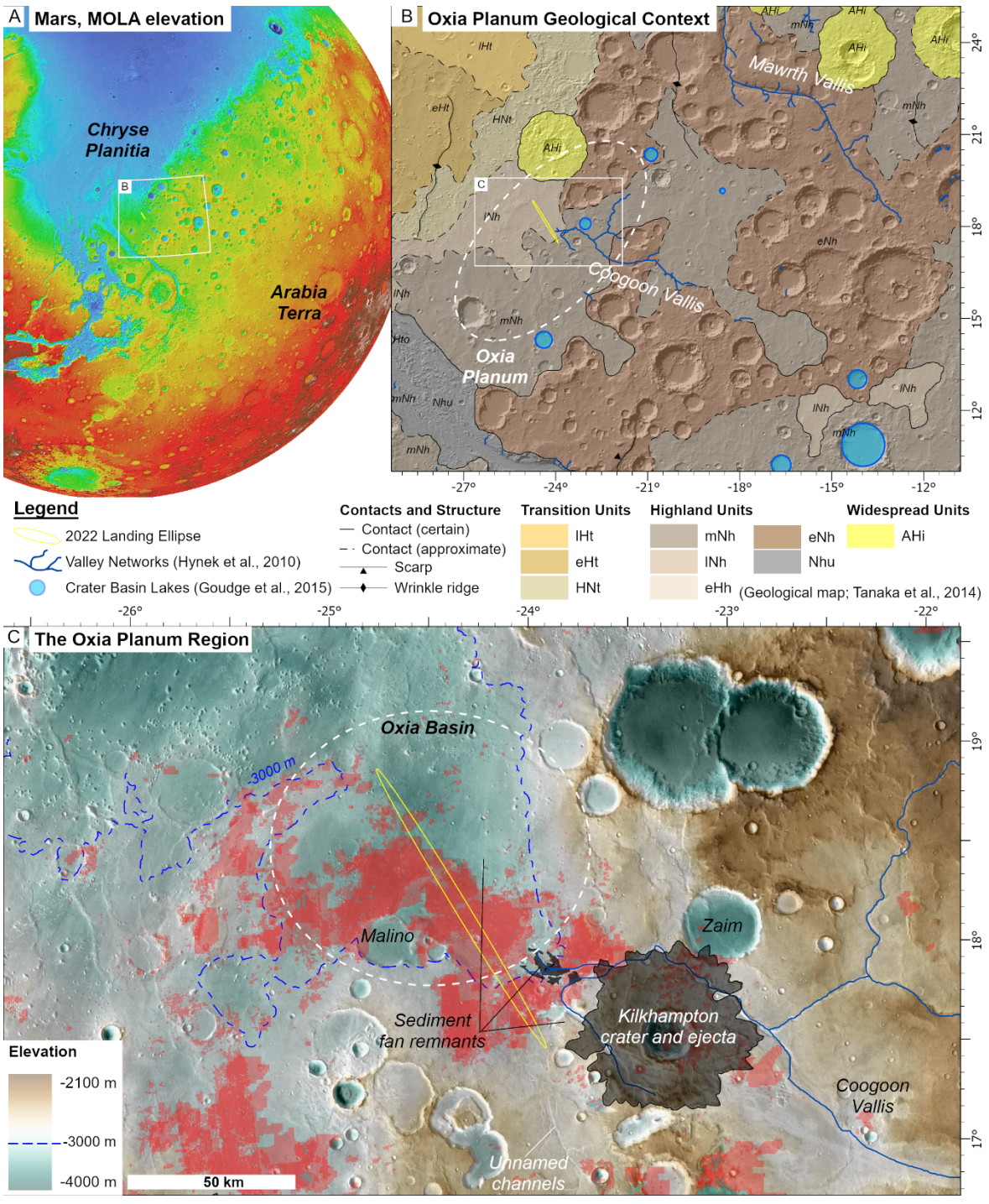
A Mars, MOLA elevation
Chryse Planitia
Arabia Terra
B
B Oxia Planum Geological Context
Mawrth Vallis
Coogoon Vallis
Oxia Planum
C
lHt
eHt
HNt
AHi
mNh
lNh
eNh
Nhu
-27°
-24°
-21°
-18°
-15°
-12°
24°
21°
18°
15°
12°
Legend
2022 Landing Ellipse
Valley Networks (Hynek et al., 2010)
Crater Basin Lakes (Goudge et al., 2015)
Contacts and Structure
Contact (certain)
Contact (approximate)
Scarp
Wrinkle ridge
Transition Units
lHt
eHt
HNt
Highland Units
mNh
lNh
eHh
eNh
Nhu
Widespread Units
AHi
(Geological map; Tanaka et al., 2014)
-26°
-25°
-24°
-23°
-22°
C The Oxia Planum Region
Oxia Basin
3000 m
Malino
Zaim
Sediment fan remnants
Kilkhampton crater and ejecta
Coogoon Vallis
Unnamed channels
Elevation
-2100 m
-3000 m
-4000 m
50 km
19°
18°
17°

Figure 1: The location of the ExoMars rover landing site at Oxia Planum (red) on: (A) Mars. (B) in context with regional geological units (Tanaka et al., 2014), previously reported 'crater lakes' and 'valley networks' (Goudge et al., 2012a, 2015a; Hynek et al., 2010). (C) The local topographic context of the 2022 landing ellipse area (3 sigma confidence landing probability ellipse shown for the opening of the launch window) in Oxia Planum including; 'The Oxia Basin', detections of phyllosilicate minerals made by the CRISM and OMEGA instruments shown in red (Quantin-Nataf et al., 2021), Coogoon Vallis (Hynek et al., 2010), the ejecta of Kilkhampton crater (grey) the -3000 m MOLA elevation contour and sediment fan remnants reported in (Molina et al., 2017; indicated by lines; Quantin-Nataf et al., 2021; black areas). Image: MOLA overlying the THEMIS day IR mosaic.

Data and Methods

2.1 Data

Geomorphological observations of fluvial features were made using CTX, 6 meter/pixel data at a scale of 1:50,000, georeferenced to High Resolution Stereo Camera MC11 quadrangle mosaic basemap (HRSC; Gwinner et al., 2016; Neukum et al., 2004). THermal EMission Imaging System (THEMIS; Christensen et al., 2013) night and daytime IR global mosaics were used to inform identification of features observed in the CTX data, and Colour and Stereo Surface Imaging System (CaSSIS; Thomas et al., 2017) images were used where available for colour interpretation. Mars Orbital Laser Altimeter (MOLA; Zuber et al., 1992) data were used for topographic information. Using these data, a fluvial (valley/channel and sinuous ridges) and lacustrine features was identified. After the initial survey, a topographic flow accumulation model was used to identify areas to revise where the model suggested channels might be present, and these were then searched more closely for any subtle morphological evidence of fluvial landforms. This iterative, multi-data process enabled many more fluvial systems to be identified than using one dataset alone. The result from this survey can be accessed in Fawdon et al., (2021)

2.2 Watershed calculation

To determine the watershed area for Oxia Planum (Figure 1), the ArcMap 10.5 Spatial Analyst 'ArcHydro' toolset (Esri, 2016) was used to calculate a model of flow accumulation grids and a drainage network map using topographic data from the MOLA DEM (Smith et al., 2001). Areas in the DEM that created sinks or basins were filled prior to calculating flow direction and accumulation. It is important to note that these processing steps 'fill in' areas of low-lying terrain and impact craters, as well as unwanted error and noise in the DEM. These 'filled in' areas create model flow pathways stretched across basins that were retained to identify where ponding may have occurred and where the model

flow is likely to deviate from the geomorphic observations.

The watershed and contributory areas were calculated using the flow accumulation model upslope of two pour points located in the *Oxia Basin*. The location of both pour points (see Figure 2) was based on the correspondence of preliminary model flow accumulation paths calculated for the whole MC-11 Quad and geomorphological features resolved in the MOLA DEM. The eastern pour point (the lowest point in the 'fan' watershed) was located where the channel of Coogoon Valles opens out into *Oxia Basin* at the highest elevation of the sediment fan remnants. The northern pour point (the lowest point in the basin watershed) was located at the lowest point of the *Oxia Basin* leading northwards to Chryse Planitia. The watershed is defined where the flow accumulation is 0 (i.e. there are no cells from which water would flow). The pour points, their watersheds, and the flow accumulation pathways were converted to Strahler stream order (Strahler, 1957) and are shown in Figure 2.

1.

Results

(a)

Reconstruction of the Palaeo-Catchment

We used surface flow accumulation model (Esri, 2016) to estimate the catchment area of the Oxia Basin and to constrain the extent of our geomorphological study. The hydrological flow accumulation calculations show a total model catchment area of 2.1×10^5 km^2 (Figure 2). This represents the total upslope area (including the *Oxia Basin*) from which water would flow over the contemporary topography though the *Oxia Basin* and northwards to Chryse Planitia. From the catchment area 71% (~1.5×10^5 km^2) accumulates into the *Oxia Basin* through the pour point labelled 'fans' (Figures 2, 3) which is coincident with remnant sedimentary fans (Molina et al., 2017; Quantin-Nataf et al., 2021). 26% (~0.6×10^5 km^2) of the catchment contributes to the *Oxia Basin* from the south (Figure 2). This area is at lower elevation with low-relief relative to the eastern part of the catchment flow, where accumulation is diverted by tectonic ridges (e.g.; Figure 1b). The remaining 3% of the catchment represents the *Oxia Basin* itself (~80 km × 80 km). This is included because it has not yet been established if the *Oxia Basin* hosted a standing body of water at any time, and whether this postulated water body was isolated from - or contiguous with - a hypothesised northern ocean (Carr and Head, 2003; Di Achille and Hynek, 2010; review by Dickeson and Davis, 2020; Parker et al., 1993).

The margins of the catchments are defined by three types of geomorphological structure (Figure 2): (i) Tectonic ridges influence model flow accumulation pathways in low-lying plains regions, particularly south of Oxia Planum and in the northwest of the catchment (Figure 2b, c). In the north of the catchment

(Figure 2b, c), a tectonic ridge that forms the boundary of the catchment is crosscut by a narrow branch of Coogoon Vallis. (ii) Throughout the catchment, impact craters form local sinks that have been filled by the watershed model (Figuer 2a). For some craters, modelled flow accumulation is concordant with the fluvial morphological features present on the surface, but for others it is discordant with fluvial features. (iii) The model flow accumulation also follows a number of early Noachian highland massifs (Figures 1b, 2c, d; Tanaka et al., 2014) with valleys on their flanks located in the south and far west of the catchment (Figures 1, 2).

Our preliminary interpretation of the model catchment is that it is generally representative of the Oxia Planum paleo-catchment, as indicated by the general concordance between the flow accumulation model, and the previously reported fluvial features in ancient highland terrains (Figure 1). However, the catchment area must be considered as a minimum estimate because there has been tectonic activity and 'modern' impact structures' which have strongly influenced the topography, and therefore affected the modelled flow accumulation. A good example is the observation showing a branch of Coogoon Vallis (as recorded in Hynek et al., 2010) traversing a modelled watershed boundary (Figure 2b) .

Figure 2: The Model Catchment of Oxia Planum

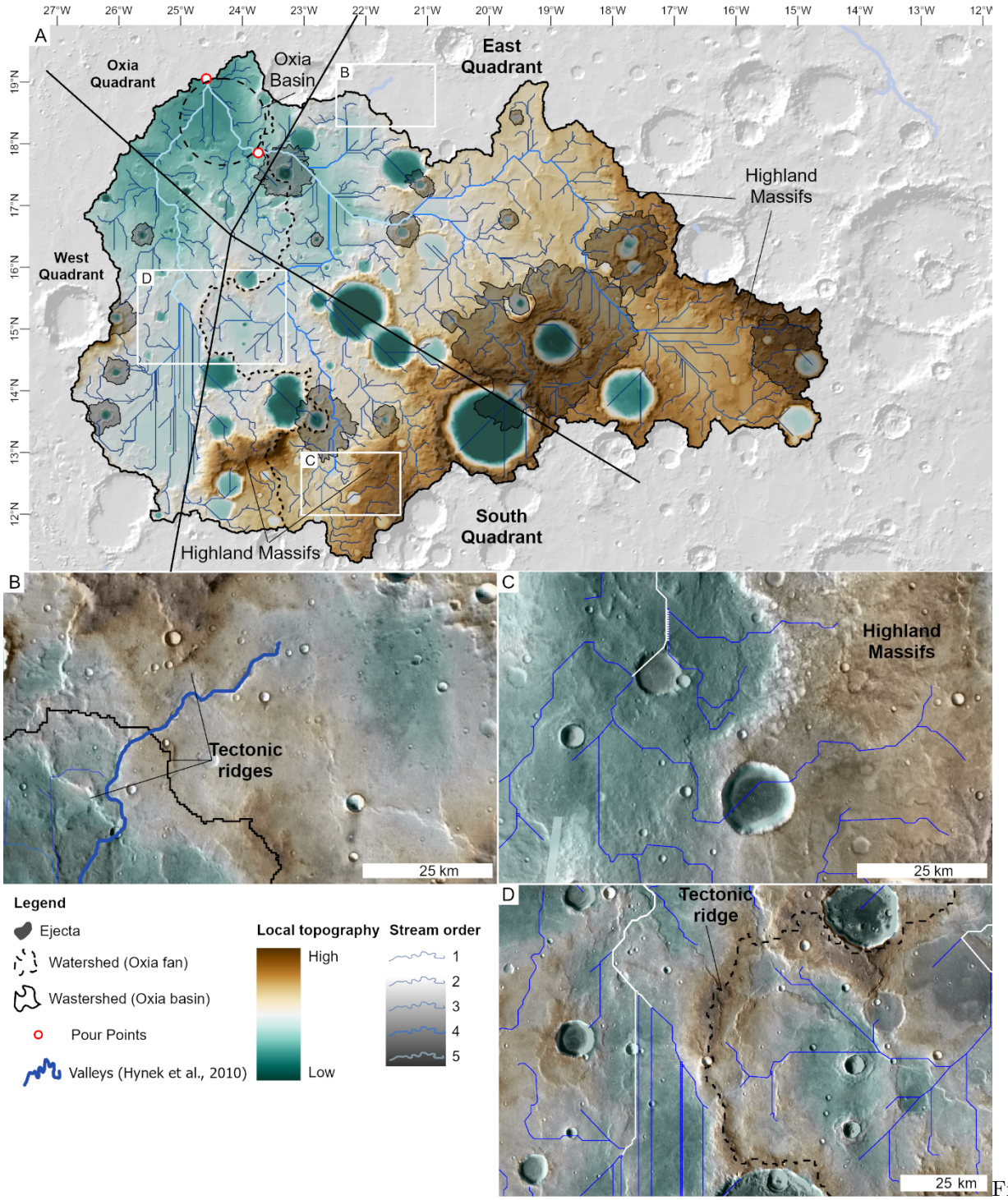
A
Oxia Quadrant
Oxia Basin
East Quadrant
Highland Massifs
West Quadrant
South Quadrant
Highland Massifs
B
C
D
Tectonic ridges
25 km
Highland Massifs
25 km
Tectonic ridge
25 km
Legend
Ejecta
Watershed (Oxia fan)
Wastershed (Oxia basin)
Pour Points
Valleys (Hynek et al., 2010)
Local topography
High
Low
Stream order
1
2
3
4
5

Figure

2: Model catchment results. (A) MOLA topography overlain on MOLA hill-shade showing model accumulation flow pathways within the model catchment. Flow paths are coloured by Strahler stream order (Strahler, 1957). (B) Example where modelled flow pathways (thin blue lines) and catchment boundaries (black line) do not match the location of mapped fluvial features (thick blue line) – in this case a branch of Coogoon Vallis. (C) A dendritic pattern of model flow accumulation conforming to the topography of early Noachian highland massifs (D) The model watershed between the basin and fan pour points formed from a tectonic ridge in the in the mid Noachian plains – such ridges can easily deviate from model flow accumulation paths in low-relief terrains. Images; MOLA overlain on THEMIS day IR mosaic.

3.2 Geomorphic evidence for ancient fluvial activity.

We used orbital images to explore how extensive the fluvial network that fed Oxia Planum was, and to test the veracity of the reconstructed paleo-catchment. We find evidence for 4 scales of valley/channel features in the Oxia catchment. In addition to the trunk valley Coogoon Vallis, we identify three types of incised paleochannels within the paleo-catchment area which transported water towards the *Oxia Basin*: (1) Wide flat-floored channels which are set within broad valleys in the landscape; (2) U-section channels which crosscut the older flat floor truck channel of Coogoon Vallis; (3) Low-relief channels/valleys which are the smallest features resolvable in the CTX data, and that are also often set within broad valleys in the landscape. These features are described below.

3.2.1 The relationship between Oxia Planum and the trunk valley of Coogoon Vallis

The main contributory input to the *Oxia Basin* is from the east through the Coogoon Vallis fluvial system (Figure 3a). However, the relationship between the channels/valleys, sediment fans, the flat floored part of Coogoon Vallis and Kilkhampton crater has considerable stratigraphic complexity (Molina et al., 2017).

East of Kilkhampton crater, Coogoon Vallis is a ~6 km wide, filled or flat-floored structure (which we refer to as '*Paleo-Coogoon*' Vallis; Figures; 2 and 3a, c) but this *Paleo-Coogoon* valley is not observed west of Kilkhampton crater ejecta. West of Kilkhampton crater are remnant sediment fan systems (Molina et al., 2017; Quantin-Nataf et al., 2021). These are associated with three narrow channels >1 km wide to the North- and South west of Kilkhampton crater (Figure 3d). These narrow channels (along with *Paleo-Coogoon*) are collectively named 'Coogoon Vallis' in Hynek et al 2010 but to differentiate them we name them '*North', 'central'* and *'south Neo-Coogoon*' (Figure 3a).

An important stratigraphic observation is that *North Neo-Coogoon* underlies the ejecta of Kilkhampton crater and is incised into the floor of '*Paleo-Coogoon*' Vallis (Figure 3d), therefore postdating it. This demonstrates that the system supplied water and sediment to Oxia Planum at different times and that the

sediment fan remnants in Oxia Planum are not associated with the development of *Paleo-Coogoon* which represent a substantially larger, and older, phase of fluvial activity.

Figure 3: The relationship between Oxia Planum and Coogoon Vallis

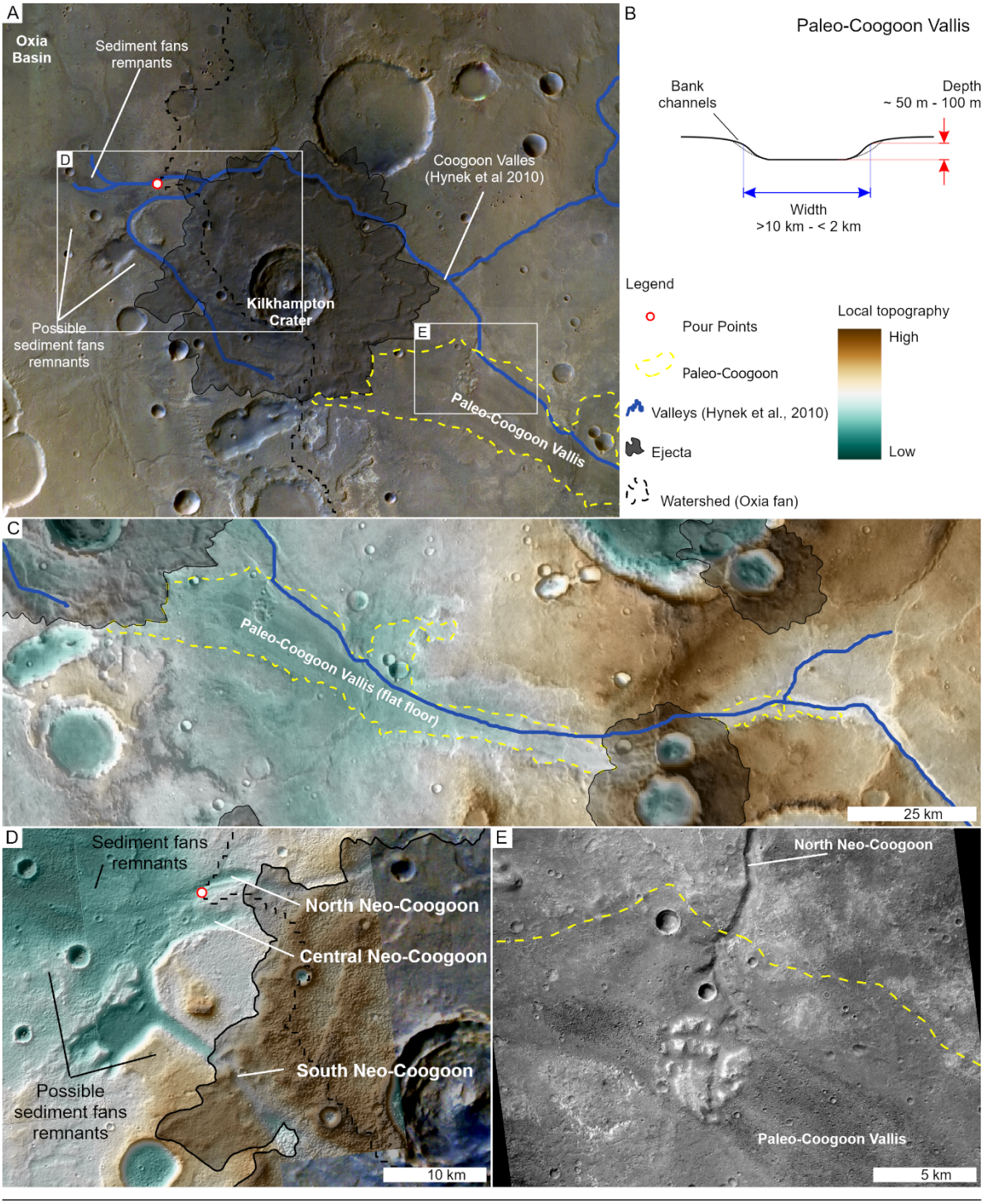
A
Oxia Basin
Sediment fans remnants
D
Coogoon Valles (Hynek et al 2010)
Kilkhampton Crater
Possible sediment fans remnants
E
Paleo-Coogoon Vallis
B
Paleo-Coogoon Vallis
Bank channels
Depth ~ 50 m - 100 m
Width >10 km - < 2 km
Legend
Pour Points
Paleo-Coogoon
Valleys (Hynek et al., 2010)
Ejecta
Watershed (Oxia fan)
Local topography
High
Low
C
Paleo-Coogoon Vallis (flat floor)
25 km
D
Sediment fans remnants
North Neo-Coogoon
Central Neo-Coogoon
South Neo-Coogoon
Possible sediment fans remnants
10 km
E
North Neo-Coogoon
Paleo-Coogoon Vallis
5 km

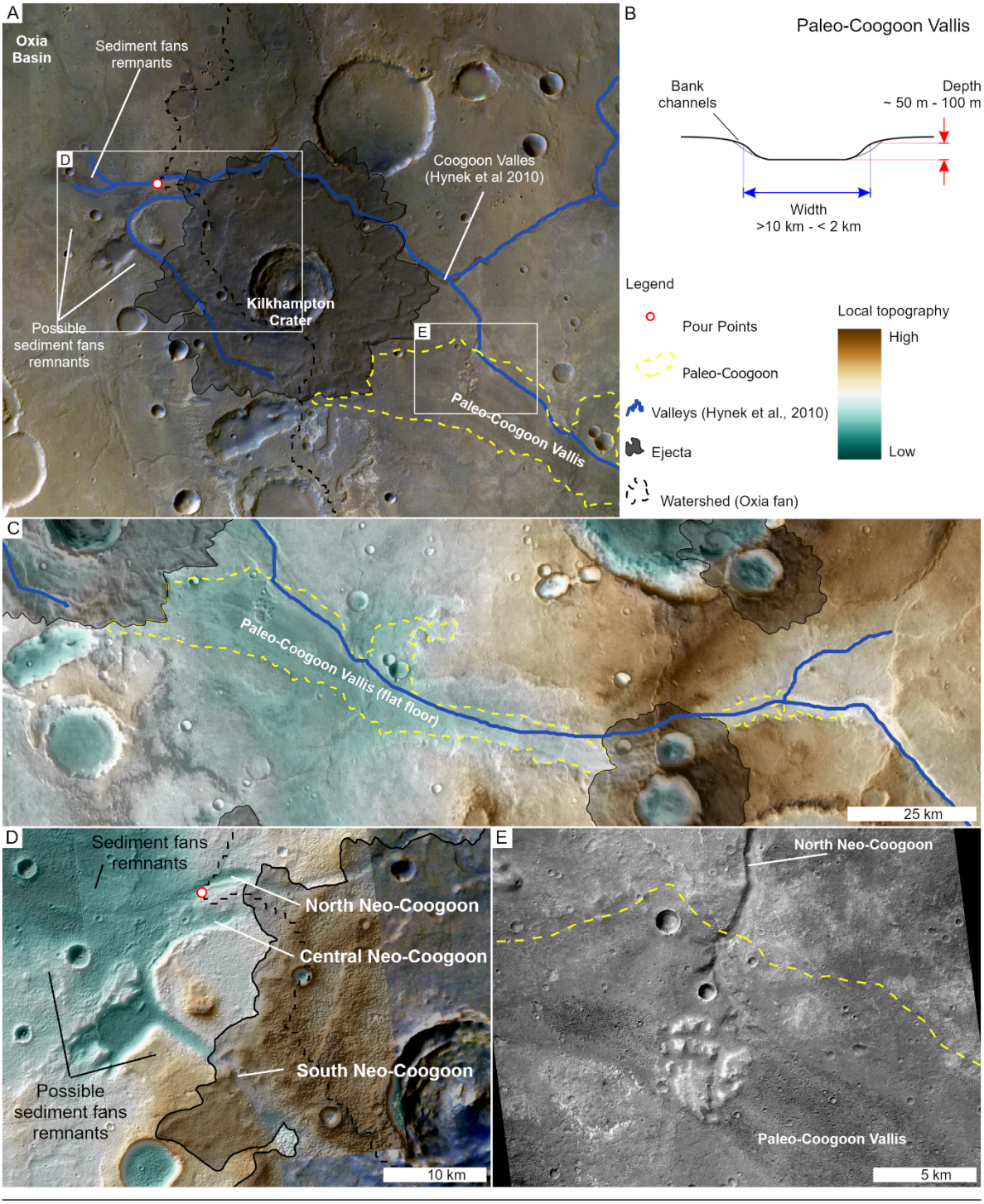
A
Oxia Basin
Sediment fans remnants
D
Coogoon Valles (Hynek et al 2010)
Kilkhampton Crater
Possible sediment fans remnants
E
Paleo-Coogoon Vallis
B
Paleo-Coogoon Vallis
Bank channels
Depth ~ 50 m - 100 m
Width >10 km - < 2 km
Legend
Pour Points
Paleo-Coogoon
Valleys (Hynek et al., 2010)
Ejecta
Watershed (Oxia fan)
Local topography
High
Low
C
Paleo-Coogoon Vallis (flat floor)
25 km
D
Sediment fans remnants
North Neo-Coogoon
Central Neo-Coogoon
South Neo-Coogoon
Possible sediment fans remnants
10 km
E
North Neo-Coogoon
Paleo-Coogoon Vallis
5 km

Figure 3: (A) The relationships between Coogoon Vallis and Kilkhampton crater showing how the western end of Paleo-Coogoon in HRSC BRG data and (B) a representative profile showing the dimensions of the Vallis. MOLA overlain on THEMIS day IR mosaic. (C) The widest flattest part of Coogoon Vallis referred to as 'Paleo-Coogoon' (D) the three Neo-Coogoon Valles are obscured by the ejecta of Kilkhampton Crater in CTX DTM data, however (E) these channels, which are 'U' shaped in profile, incise (and thus postdate) the paleo-Coogoon Vallis as seen in CTX image G01_018662_1981_XN_18N022W

3.2.2 Wide flat floored channels/valleys

Wide, Flat-Floored ('WFF') channels/valleys occur within the catchment (Figure 4a). The largest example trends east from the trunk valley Palaeo-Cogoon Vallis (Figure 3c) where this channel is ~5 km in width and up to 150 m deep. (Figure 3, 4). To the east the channel narrows up slope to ~1 km in width and ~50 m in depth where it is intersected by subsidiary channels at high junction angles. Down slope, towards Oxia Planum, this channel opens out, and the margins become less distinct. Here, it is >10 km in width with a smooth floor that appears to be infilled by a younger dark-toned unit. Other wide (>1 km) channels with shallow banks elsewhere in the catchment are much less extensive. Wide flat floored channels lie in valleys which conform to the long wavelength (10's km) topography of the catchment (Figure 4c).

3.2.3 U-section channels

U-section channels are found in the northwest of the model catchment (Figure 4a). They are generally ~50 m to 100 m in depth (Figure 4) and ~ 500-1000 m wide. Their topography is significant enough to be captured in the flow accumulation model results. U-section channels incise the valleys of wide flat floored channels and their upslope terminations are often abrupt, forming 'amphitheatre' shapes (figure 4; G to I). Unless crosscutting the floor of an older channel, U-section channels are not situated within their own valleys (Figure 4). U-section terminations often trend into Low-relief Channels/valleys (section 3.2.4) upslope. In some cases, u-section have been deformed by later tectonic activity (Figure 2c).

The cross-cutting relationships show that u-section channels were active after landscape modification associated with the Palaeo-Coogoon channel. U-section channels appear to be superimposed on this older landscape, reactivating the older flow pathways; their relatively straight courses and sharp terminations (figure 4; G to I) suggest that they were not active for long enough to equilibrate with the pre-existing topography. U-section channels predate the most recent stages of regional tectonic deformation (Figure 2b), so the elevation of their terminations, and their present-day topographic long-profiles, might not reflect their original elevations when they were active.

Figure 4: Wide flat floored and u-section channels

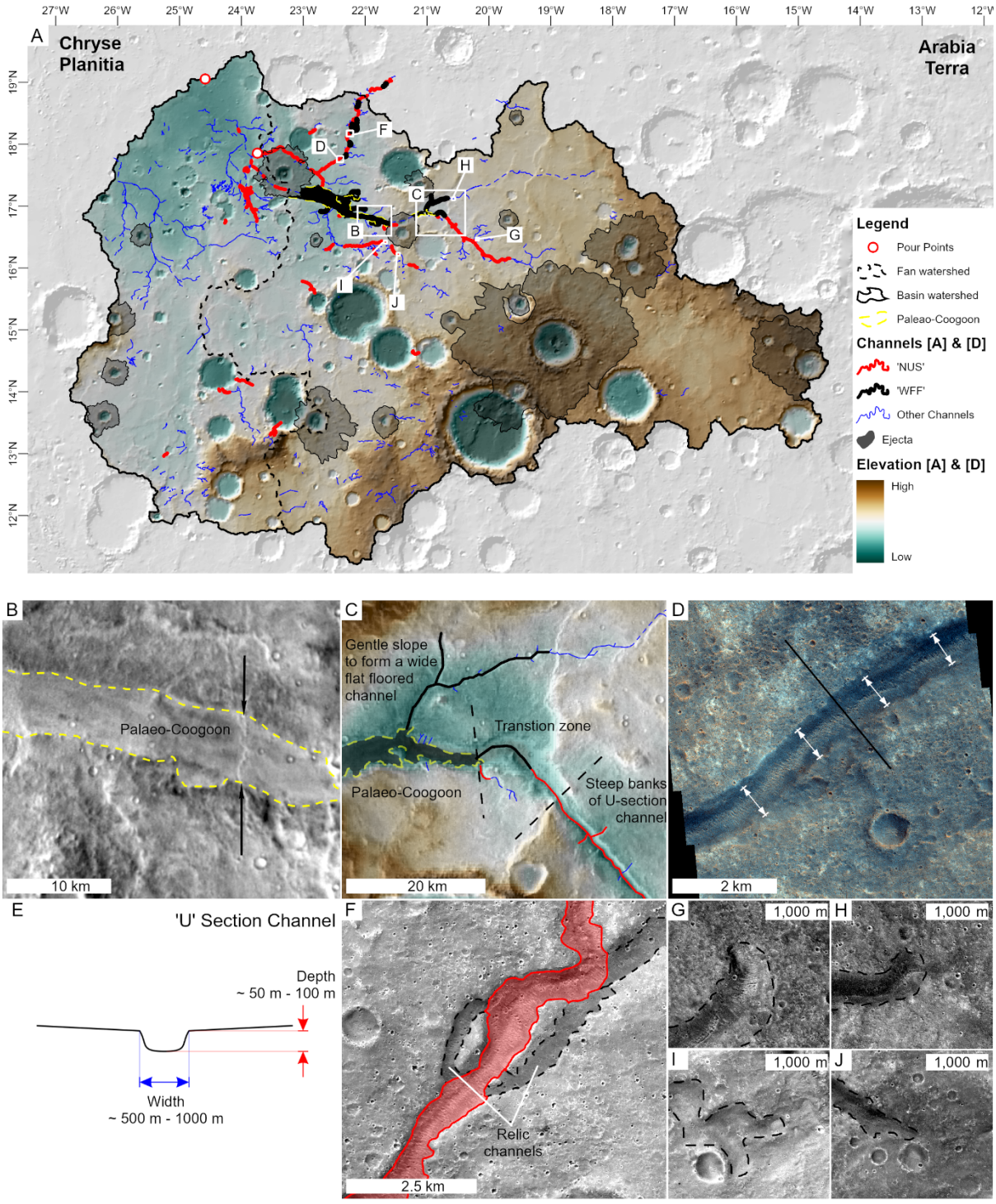
A
Chryse Planitia
Arabia Terra
27°W
26°W
25°W
24°W
23°W
22°W
21°W
20°W
19°W
18°W
17°W
16°W
15°W
14°W
13°W
12°W
19°N
18°N
17°N
16°N
15°N
14°N
13°N
12°N
D
F
H
C
B
G
I
J
Legend
Pour Points
Fan watershed
Basin watershed
Paleao-Coogoon
Channels [A] & [D]
'NUS'
'WFF'
Other Channels
Ejecta
Elevation [A] & [D]
High
Low
B
Palaeo-Coogoon
10 km
C
Gentle slope to form a wide flat floored channel
Transtion zone
Palaeo-Coogoon
Steep banks of U-section channel
20 km
D
2 km
E
'U' Section Channel
Depth
~ 50 m - 100 m
Width
~ 500 m - 1000 m
F
Relic channels
2.5 km
G
1,000 m
H
1,000 m
I
1,000 m
J
1,000 m

Figure 4: The distribution of linear features interpreted from CTX imagery to be fluvial landforms in the region of the model catchment. (A) The distribution of Wide Flat Floored (WFF) and Narrow U-Section (NUS) channels (for other channel-like landforms see Figure 5). (B) The smooth floor of 'Paleo-Coogoon' Vallis is crosscut by a tectonic ridge (arrowed). (C) The Complex transition between 'Paleo-Coogoon', 'normal' wide flat floored channels and u-section channels showing the shallow banks associated with wide flat floored channels and the steep banks associated with u-section channels. (D) CaSSIS image (MY34_006975_165_0) showing a typical section of u-section channel ~1 km in width incising light toned bedrock north of Coogoon Vallis. (E) a representative cross-section shows the typical dimensions of a u-section channel. (F) u-section channel incising into a set of pre-existing channels with shallower banks, leaving those channels hanging in the main channel wall. (G-J) CTX data showing four examples of amphitheatre-like origin points of u-section channels (although mantling material obscures clear contacts).

3.2.4 Low-relief channels

Low-relief channels (LRC; Figure 5) incise plains materials (Figure 1b; unit mNh) throughout the model catchment. They range in width from ~500 m to less than ~100 m and their depths are estimated to be <10 m based on the limited CTX DTM coverage. At length-scales smaller than this, the expression of low-relief channels becomes muted and it is no longer possible to clearly observe them. Low-relief channel generally occur as upslope continuations of u-section and wide flat floored channels, or as lower order branches that feed into u-section or wide flat floored channels. Low-relief channel are also often observed upslope of amphitheatre shaped onset points of u-section channels (Figure 4). Low-relief channel have a low sinuosity often branch up slope into smaller channels (Figure 5d) and also trend into (and from) low-relief sinuous ridges (Figure 6)

Low-relief channels represent the smallest, narrowest channels in the network that formed contemporaneously with wide flat-floored valleys. Low-relief type channels were probably subsequently reactivated in association with the development of the u-section channels as they are observed to merge into channels of this type. We interpret that the minimum observable size is related to the effects of erosion (e.g. by wind and small scale impacts (Golombek et al., 2014)) and burial or regolith development since they were last active. Where low-relief channels trend into sinuous ridges, this suggests that that these channel were part of an aggregational alluvial system, so they have deposited sediment in places and did not just incise a pre-existing surface.

Figure 5: Low-relief channels

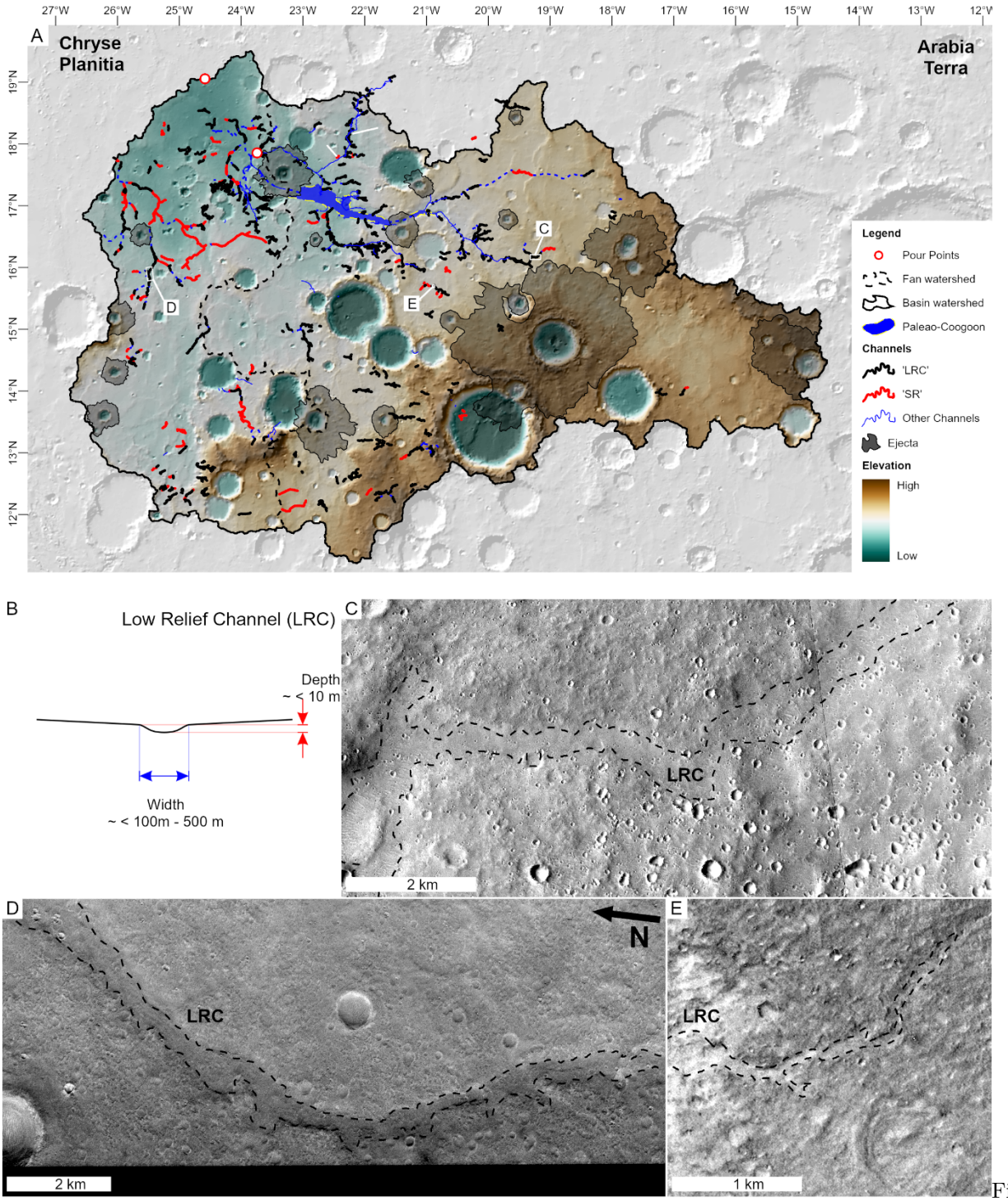
A
Chryse Planitia
Arabia Terra
27°W
26°W
25°W
24°W
23°W
22°W
21°W
20°W
19°W
18°W
17°W
16°W
15°W
14°W
13°W
12°W
19°N
18°N
17°N
16°N
15°N
14°N
13°N
12°N
C
D
E
Legend
Pour Points
Fan watershed
Basin watershed
Paleao-Coogoon
Channels
'LRC'
'SR'
Other Channels
Ejecta
Elevation
High
Low
B
Low Relief Channel (LRC)
Depth
~ < 10 m
Width
~ < 100m - 500 m
C
LRC
2 km
D
N
LRC
2 km
E
LRC
1 km

Figure

5: The distribution of linear features interpreted from CTX imagery to be to be fluvial landforms in the region of the model catchment. (A) The distribution of Low-relief Channels (LRC; Black) and Sinuous Ridges (SR; Red) (for other channel-like landforms see Figure 4). (B) representative cross-section showing the typical dimensions of low-relief channel channels. (C) and (D) show examples in CTX data of low-relief channel and becoming narrower and muted upstream to the east. (E) A subtle low-relief channel branching into smaller less visible channels. Images show CTX data.

3.2.5 Sinuous Ridges

In addition to the network of incised channels, a network of sinuous ridges are found in the west of the catchment (Figures 5a, 6). Sinuous ridges are up to ~500 m in width, are estimated to be up to 10 m in height and often form as continuations of low-relief channel channel forms. Sinuous ridges are found in areas with 'inverted' crater fills and eroded remnant mounds (McNeil et al., 2021). This suggests that substantial burial and erosion has occurred. Sinuous ridges are also associated with light toned fractured terrains. Sinuous ridges exhibit branching patterns (Figure 6e), as well as a variety of surface textures, and are overlain by the regionally significant rounded buttes (Figures 6e) part of a significant regional population (McNeil et al., 2021).

We interpret the sinuous ridges as inverted fluvial channel deposits (e.g; Figures; 5a,6; Pain and Ollier, 1995) comparable to similar features seen throughout western Arabia Terra (e.g., Balme et al., 2020; Davis et al., 2019, 2016; Day et al., 2019; Edgett and Malin, 2002; Newsom et al., 2010; Williams et al., 2009). We attribute the variation in occurrence to regional variations in exhumation processes and degree of erosion. To the north-west of the catchment where there has been the most erosion, sinuous ridges predate the formation of the rounded buttes (Figure 6e) which are likely to have been part of a regionally extensive layer (McNeil et al., 2021). This means the material of the ridges (i.e. fossilised stream beds, assuming the widely accepted interpretation) are at a similar stratigraphic level to the clays (lNh, mNh; Figure 1) that comprise Oxia Planum (Fawdon et al., 2021 submitted; Mandon et al., 2021; Parkes-Bowen et al., 2021; Quantin-Nataf et al., 2021) consistent with other inverted channel systems in the region (e.g.; Balme et al., 2020; Marzo et al., 2009)

Figure 6: Sinuous Ridges

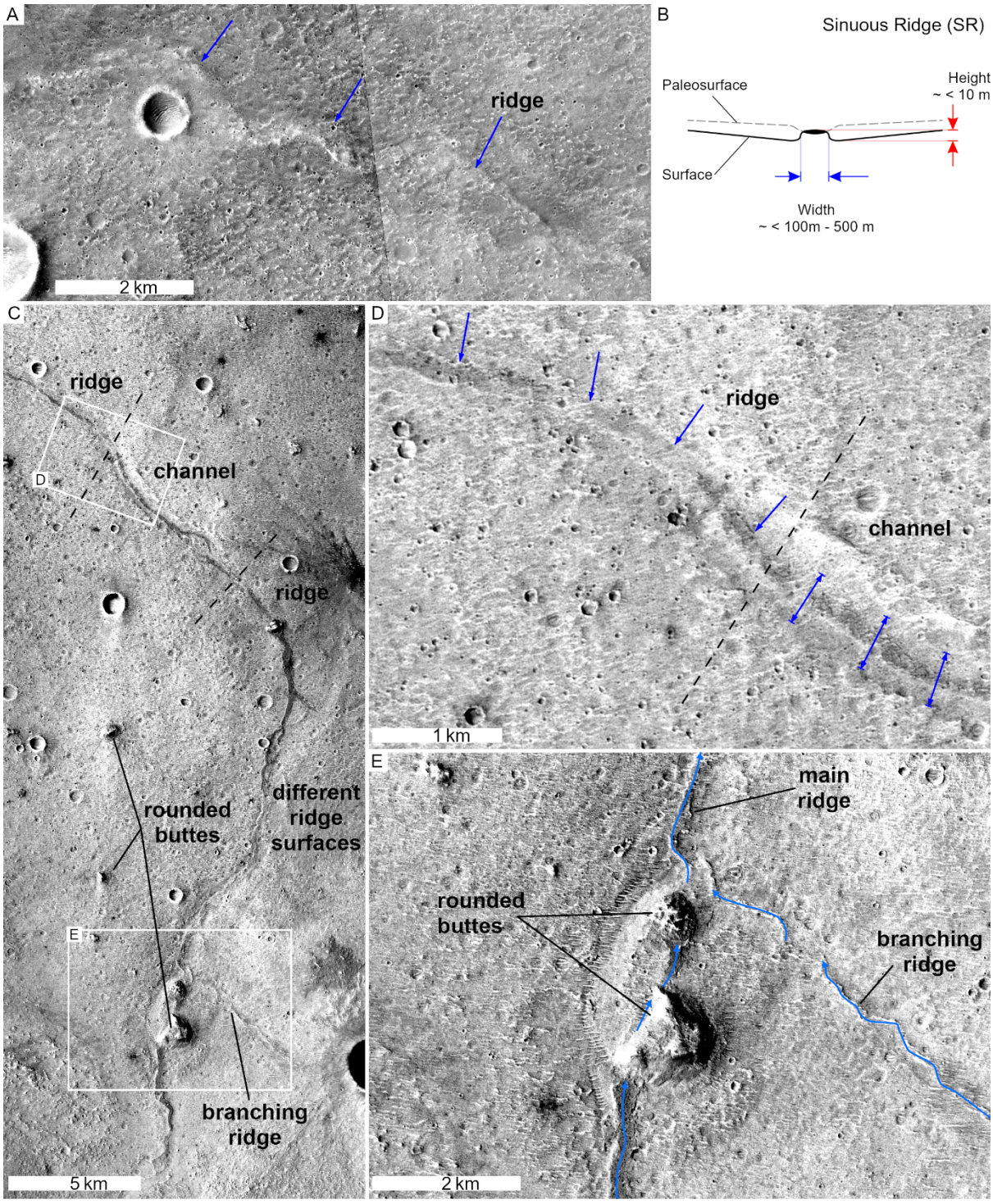
A
ridge
2 km
B
Sinuous Ridge (SR)
Paleosurface
Height
~ < 10 m
Surface
Width
~ < 100m - 500 m
C
ridge
channel
D
ridge
rounded
buttes
different
ridge
surfaces
E
branching
ridge
5 km
D
ridge
channel
1 km
E
main
ridge
rounded
buttes
branching
ridge
2 km

Figure 6: A Sinuous Ridge (SR) in (a) the eastern part of the catchment and (b) the typical dimensions of sinuous ridges in the catchment. (c) A stretch of a sinuous ridge in the eroded landscape of the west quadrant of the catchment (Figures 2, 5) showing the divers landforms associate with sinuous ridges. Here (d) the plains subjacent of sinuous ridges transition into valley or low-relief channel, the sinuous ridges have different texture on their top surface. (E) branching sinuous ridges are overlain by rounded buttes (McNeil et al., 2021). All images use CTX data.

3.3 Geomorphic evidence for paleolakes in the region of the model catchment area

Within the model paleo-catchment, 180 locations show possible evidence of liquid water having ponded in the past as 'paleolake basins'. The strongest evidence to support a paleolake basin interpretation is the presence of a topographic basin associated with an overspill outlet channel (e.g. Figure 8) which suggests that water once filled the basin to at least the level of the overspill (e.g., Goudge et al., 2012a). A variety of other landforms are often observed in these paleolake basins (Cabrol and Grin, 1999; Fassett and Head III, 2008; Goudge et al., 2012a, 2015a; Wharton et al., 1995) in addition to overspill channels, so we also used the following evidence to infer the presence of paleolakes: (1) smooth layered crater floor deposits not associated with evidence for volcanic architecture (Cabrol et al., 2003; Hauber et al., 2011); (2) sediment fans (e.g.; Goudge et al., 2015a; Hauber et al., 2009; Palucis et al., 2014); (3) presence of interior crater wall channels with circumferential interior crater wall slumps and (4) possible strandlines (e.g.; Cabrol and Grin, 1999; Deit et al., 2013; Komatsu et al., 2001; Ori et al., 2000; Salese et al., 2019).

We compiled an initial catalogue of possible paleolake locations from impact structures identified by (Robbins and Hynek, 2012a, 2012b), our survey of the THEMIS and CTX data and locations where the slope of a 'filled' (Esri, 2017; Planchon and Darboux, 2002) MOLA DEM was 0°. We consider possible paleolakes as any location that exhibited at least one of these pieces of morphological evidence for ponded water when found in association with a plausible topographic context. We also consider CRISM/OMEGA observations associated with geomorphic evidence (Carter et al., 2015; Wray et al., 2011) as supporting evidence for lake activity when identified in context with an assemblage of the other landforms. Based on the presence of these landforms, the degree of evidence for ponded water and their size, we have divided the possible paleolake basins in the model catchment (Figure 7) into three classes: (1) Large Crater Lakes (LCL; Figure 8); (2) Rimless Crater Lakes (RCL; Figure 9); and (3) Irregular Dark Depressions (IDD; Figure 10).

Figure 7: Distribution of Channels and lakes

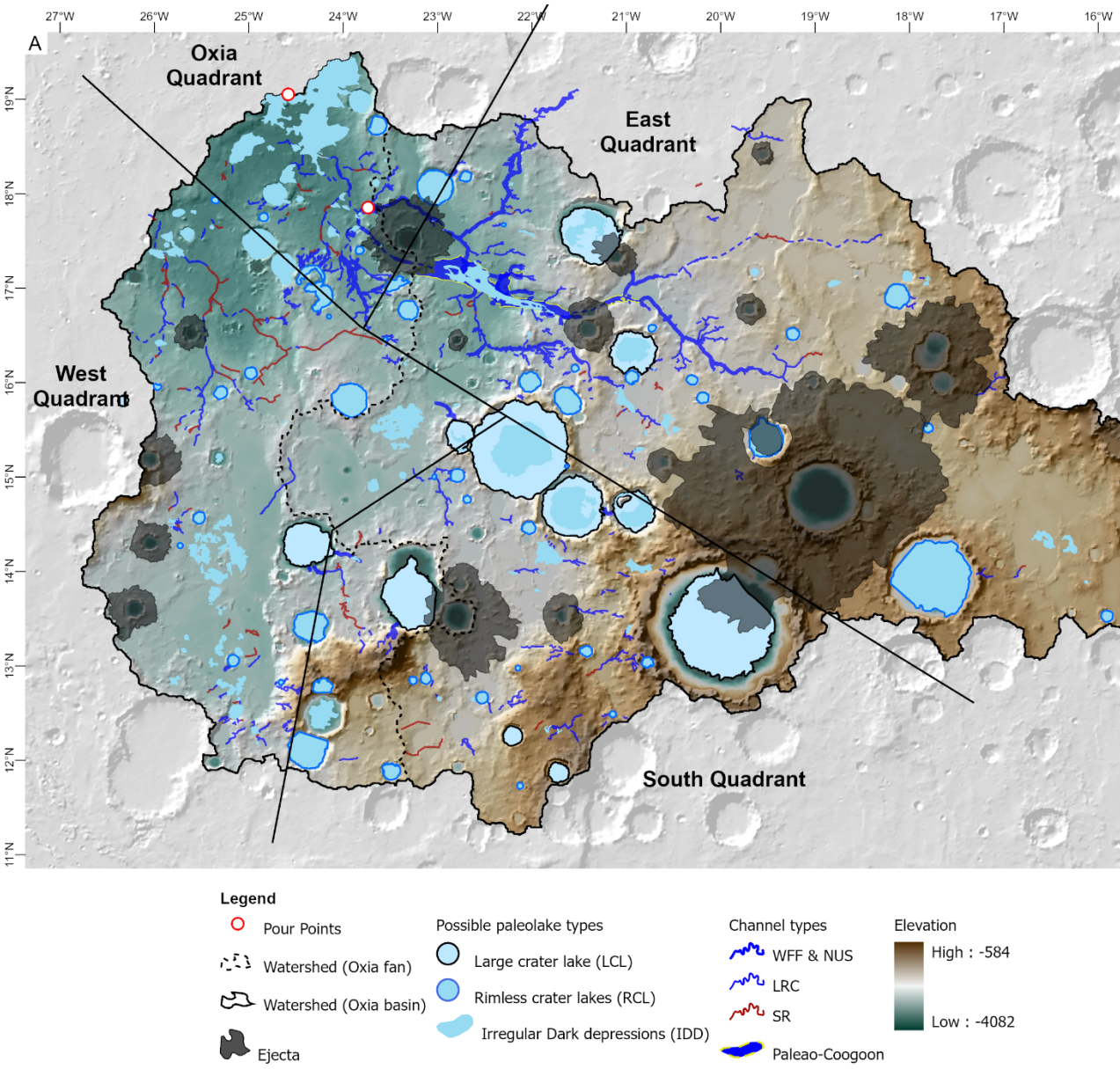

Figure 7: The distribution of possible paleolakes and fluvial pathways in the model catchment of Oxia Planum.

3.3.1 Large Crater Lakes

Large Crater lakes (LCL; Figure 8) are the class of larger impact crater which show the most compelling evidence for being ancient lakes. They have a mean

area of ~1100 km^2 and mean diameter of ~33 km and retain an upstanding crater rim. Of the 12 examples observed in this class, eight have identifiable inlet valleys and four of these also have outlet channels exiting the crater. Large crater lakes also often (8 of 12 examples) have channels on the inside of their crater walls (Figure 8b). Four examples of large crater lakes form in a chain of craters (Figure 8). In this chain, the western-most crater has an outflow channel (Figure 8c), the eastern most crater has inlets from highland to the south-west and outlets to one of the central craters (Figure 8d), although this is not directly connected to the largest crater in the chain. On the smooth flat floor of this largest crater there is an erosional window up to 150 m deep revealing sharply defined, sub-horizonal layers with a mean thickness of 6 m (Figure 8e).

The presence of Inlet and outlet channels show that many of these craters hosted at least one instance of a lake. The layered deposits on the floor of one crater, in which Carter et al. (2015) identified the spectral signatures of phyllosilicate minerals, give us confidence that similar floor morphologies (i.e. all large crater lakes and rimless crater lakes) are also likely to constitute aqueously altered sedimentary deposits. Where large crater lakes do not have outflow channels but do have interior channels predominantly below the elevation of the surrounding plains. We interpret this morphology to have formed by flow of water through the crater walls, because the groundwater table was likely above the crater floor. Consequently, several instances of progressively shallower high stands and lake depths could form with fluctuating groundwater levels without breaching the crater rim. No evidence of volcanic architecture was seen to suggest the craters were flooded by lava.

Figure 8: Large crater lakes

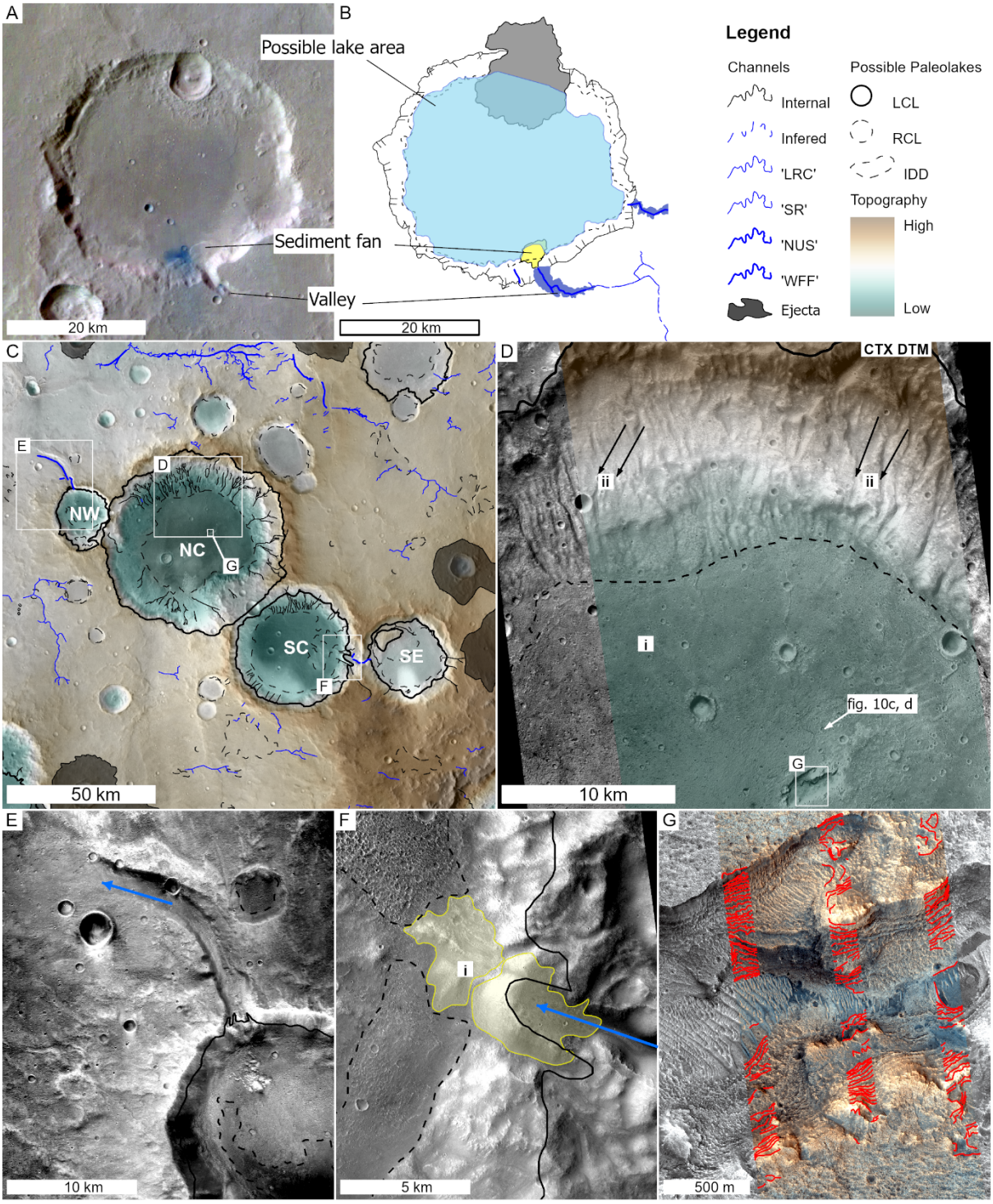
A
B
Possible lake area
Sediment fan
Valley
20 km
20 km
Legend
Channels
Internal
Infered
'LRC'
'SR'
'NUS'
'WFF'
Ejecta
Possible Paleolakes
LCL
RCL
IDD
Topography
High
Low
C
E
D
NW
NC
G
SC
SE
F
50 km
D
CTX DTM
ii
ii
i
fig. 10c, d
G
10 km
E
10 km
F
i
5 km
G
500 m

Figure 8: Examples of Large Crater Lakes (LCL) (A) in HRSC colour data and (B) as an illustrative sketch showing the crater rim, sediment fan (yellow), possible area of the lake (blue), area of the inlet valleys and channels (dark blue) and impact ejecta that postdates the crater floor (grey). (C) The chain of four craters (North West; NW, North Central; NC, South Central; SC, South East; SE). (D) The (i) smooth floor, (ii) interior channels in large crater lake NC. Black line indicates the outlet elevation into crater NW (E) and black dashed line indicates edge of the Irregular Dark Depression of the smooth crater floor. (F) An example of sediment fans connecting craters SE and SC. Black and dashed lines indicate possible high and low water stands. (G) HiRISE image (ESP_059448_1955) showing A ~150 m deep window showing the layered structure of the phyllosilicate bearing NC crater floor. Red lines identify ~6m thick layers in in three transects.

3.3.2 Rimless Crater lakes

Rimless Crater lakes (RCL) are a class of smaller basins that are flat-floored, quasi-circular depressions with little or no topographic rim (Figure 9). Some also have inflow and or outflow channels (only 17/52 examples; figure 9a). The floor of rimless crater lakes are often smooth (32/52 examples) at scales of hundreds to thousands of meters, and the interior wall or floor close to the interior crater wall often (34/52 examples) have small topographic steps or breaks in slope that ring the basin at an approximately consistent elevation (figure 9c).

We created 24 crater rim-floor profiles, extracted from 100 m/pixel HRSC DEM (Gwinner et al., 2016) data, of six rimless crater lakes basins and six other proximal (within <100 km) 'reference' craters that do not appear to have hosted lakes. All examples are ~10 km in diameter (figure 9d). The profiles show that rimless crater lakes craters have lost ~200 m of rim height and 600m from the rim to floor depth compared to the reference crater population, which did not host any paleolake criteria morphologies. Accounting for the change in rim height the rimless crater lake basins also have been infilled by ~300 - 400 m of material not present in other craters in the same geographic area.

We interpret rimless crater lakes to be the remnants of substantially degraded impact craters where the majority or all of the impact crater rim has been removed and the floor infilled by hundreds of meters of material. The removal of the crater rim is consistent with them being part of a mature (Craddock et al., 2018) mid-Noachian landscape (Craddock and Maxwell, 1990).

We interpret the smooth flat floors and interior topographic steps/breaks in slope as 'strand lines' indicating deposition conforming to an approximately equipotential surface. Where these features are found in association with inlet channels and sediment fans, we are confident that the rimless crater lakes have hosted instances of paleolakes at some point in their history. The lack of outlets associated with rimless crater lakes means they did not overflow and are not connected by overland flow into the regional fluvial systems (Section 3.2). This

means lake depth and longevity is likely to have been controlled by the depth of the crater and height of the groundwater table.

Figure 9: Rimless crater lakes

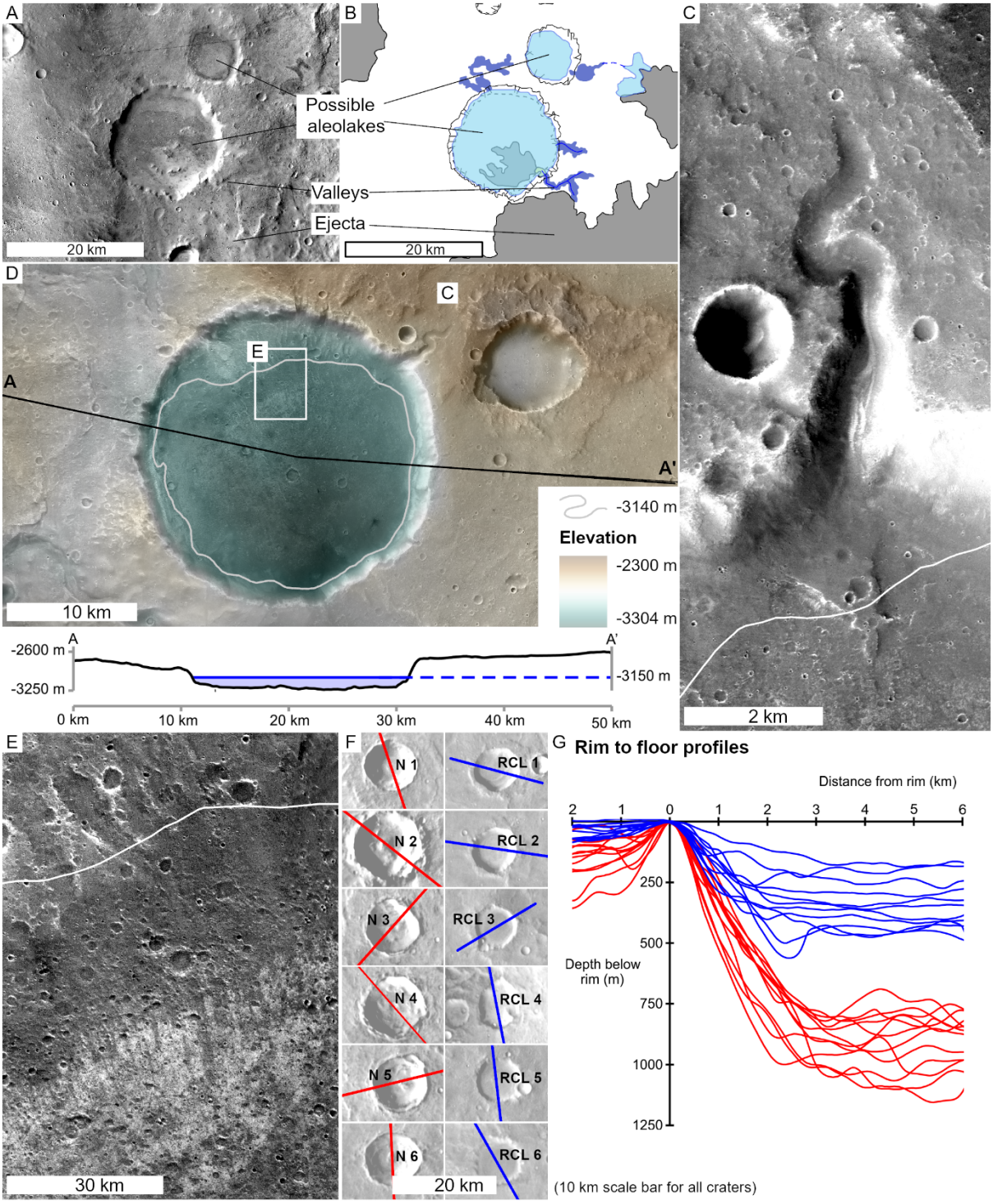
A
B
C
Possible
aleolakes
Valleys
Ejecta
20 km
20 km
D
C
E
A
A'
-3140 m
Elevation
-2300 m
-3304 m
10 km
2 km
A
A'
-2600 m
-3250 m
-3150 m
0 km
10 km
20 km
30 km
40 km
50 km
E
F
G
Rim to floor profiles
Distance from rim (km)
2
1
0
1
2
3
4
5
6
250
500
750
1000
1250
Depth below
rim (m)
N 1
N 2
N 3
N 4
N 5
N 6
RCL 1
RCL 2
RCL 3
RCL 4
RCL 5
RCL 6
30 km
20 km
(10 km scale bar for all craters)

Figure 9: Examples of Rimless Crater Lake (RCL) (A) in HRSC colour data and (B) as an illustrative sketch showing the crater rim, possible area of the lake (blue), area of the inlet valleys and channels (dark blue) and impact ejecta that postdates the crater floor (grey).Features and topography of (C) Zaim a rimless crater lakes which include the complete erosion of the crater rims, smooth flat floors and inlet channels associated with a valley system. (D) Cross section of Zaim crater showing the removed rim, flat crater floor and the elevation of the sediment fan. (E) Sediment fan and part of the inlet valley, whilst it is not possible to make interpretations of this fan it can be taken as a maximum possible water level. (F) Smooth floor materials on lapping channels in the interior of Zaim crater at a constant topographic level. (G) 24 crater wall profiles from 12 craters, 6 identified as rimless crater lakes from morphology other than topography and the closest 6 'normal' craters of a similar diameter.

3.3.3 Irregular dark depressions

The most numerous class of potential paleolake landforms are irregular dark depressions (IDD; Figure 10). In CTX images, these terrains are predominantly dark in tone and occur either on the floor of impact craters associated with rimless crater lakes or large crater lakes (Figure 4a, b) or in topographic lows in intercrater plains. Where irregular dark depressions occur in inter-crater plains they are often associated with channels or sinuous ridges. The best example of this (Figures 7f, 10a,b) has one very clear outlet which leads to Coogoon Vallis, and several possible inlet channels or sinuous ridges. The margins of irregular dark depressions appear to follow specific contours unless they have been crosscut by tectonic ridges, and often show concentric albedo bands at their margins. These bands comprise a bright fringe at the edge of the feature, and a darker band inside, which transitions to a tone comparable to that of the surrounding plains in the centre of the feature. There is often a topographic step at the edge of each of these bands, which appears bright in night time THEMIS data. This is most noticeable where irregular dark depressions are also found in association with sinuous ridges (e.g. Figure 6). Where HiRISE image data and CTX topographic data are available (Figure 10c, d) the darker irregular dark depression material has distinct layers (Figure 10d) and forms a sharp boundary with the underlying light-toned, clay-bearing crater floor material (see figure 8).

We tentatively interpret the irregular dark depressions recorded in this study as paleolake or playa deposits based on their location in the topography, and their association with the regional network of channels and ridges. We interpret the dark deposit to be dark previously unconsolidated transported material cemented in local topographic lows at times of high stand of the groundwater table. We attribute the concentric bright and dark rims to be this darker capping material and a brighter, less erosion resistant underlying material that is undergoing a terrain inversion process. However, there are many processes that could produce these features, and many examples of dark materials in different contexts that are not associated with topographic lows for which we do not explore an

interpretation. For example, similar features have previously been interpreted as remnants of mega-tsunami runout deposits (Rodriguez et al., 2016) or, because of their pyroxene-dominated minerology, as volcanic deposits (Ivanov et al., 2020; Quantin-Nataf et al., 2021).

Figure 10: Irregular Dark Depressions

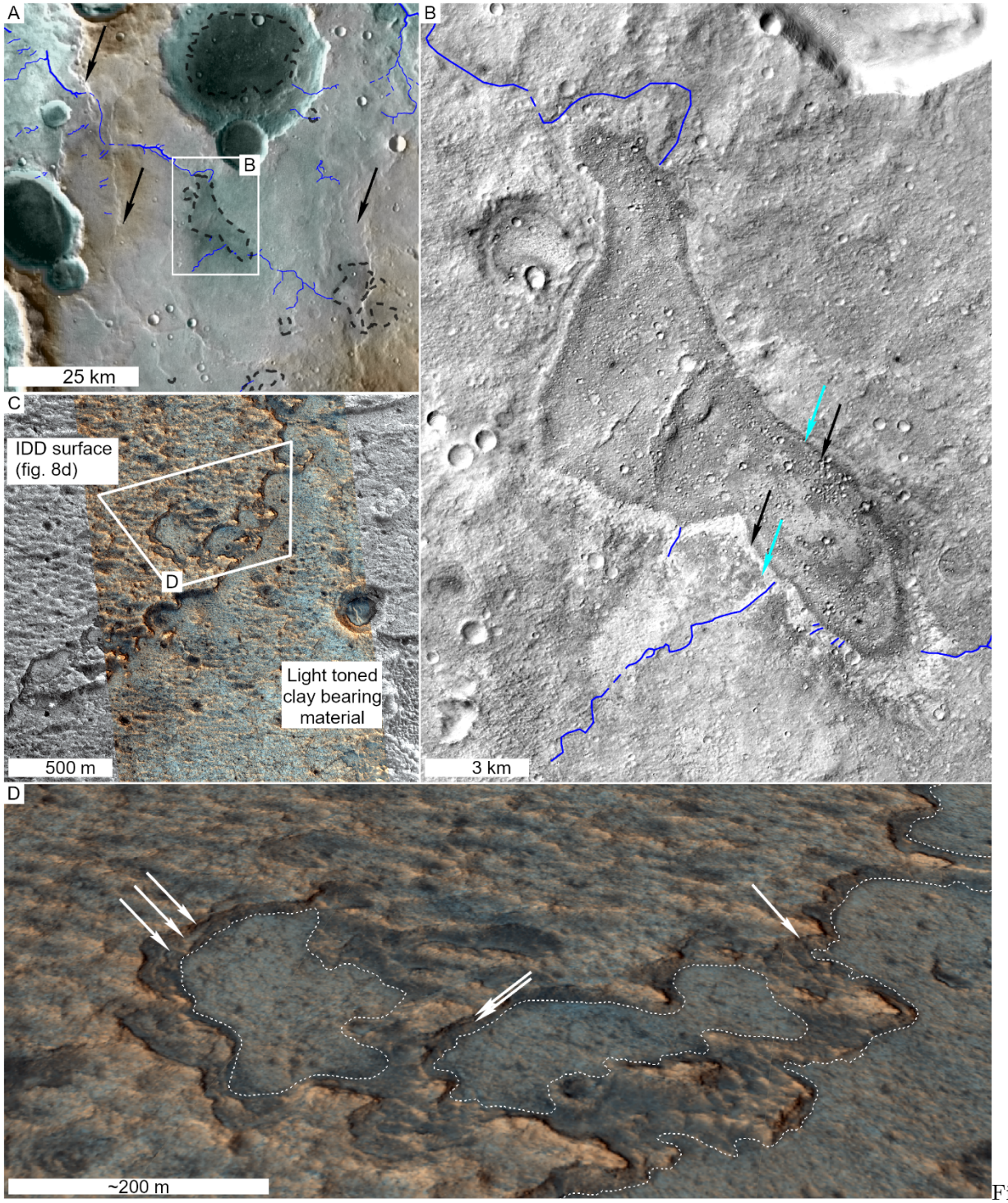
A
B
25 km
B
3 km
C
IDD surface
(fig. 8d)
D
Light toned
clay bearing
material
500 m
D
~200 m
Figure

10: Topographic context (A) of an intercrater irregular dark depression (IDD), the irregular dark depression sits in a local topographic low although this contemporary topography shows the associated channel system (blue) has been crosscut by ~N-S trending tectonic ridges (white arrows). (B) CTX image of the irregular dark depression showing the concentric light and dark toned rim and association with various low-relief channels and sinuous ridges (SR: blue lines). (C) A shallow erosion pit (figure 9) shows the edge of the irregular dark depression material on the floor of a large crater lake. (D) A perspective view showing the layering in the thin (<5 m) irregular dark depression deposit overlying the light-toned clay-bearing material (Figure 8).

3.3.4 Distribution of channels and lakes

The distribution of channels and possible paleolakes (Figures 4a, 5a 7) approximately divides the region into zones based on the pattern of fluvial and lacustrine features in the landscape. In the Eastern Zone channels form dendritic patterns branching out from Coogoon Vallis. When traced upslope, the channels transition in morphology from wide flat-floored to low-relief-channels, or from wide flat-floored to u-section and to low-relief channels with the u-section channels superposing the wide flat-floored channels (Figure 4). The topography of the east quadrant slopes down towards the channels but the paleolakes generally occur at higher elevations. In the Southern Zone the channels are predominantly low-relief channels and form a discontinuous pattern. The trends of this pattern are associated with the slopes of the mid Noachian (Figure 1) highland massifs to the south of the quadrant. In the Western Zone the topography forms a low-lying and low-relief plain that is crosscut by the regional north-south tectonic fabric, and here the craters are often infilled or 'ghost' craters picked out by the ridges. To the north of the West zone, a network of contributory low-relief channel and sinuous ridges extend out of the model catchment south of Oxia Planum, whilst in the south, numerous irregular dark depressions appear to be constrained by the tectonic ridges. In the centre of the catchment (the east of the West Zone) is a large irregular dark depression associated with outflow from the central chain of craters (Figure 8) and u-section channels in the south of the Oxia Zone. The Oxia Zone, containing the ExoMars landing site is a shallow basin (Figures 1, 7) is located at the confluence of drainage from the East and West Zones. The *Oxia Basin* is fed from the East zone by Coogoon Vallis, u-section channels which superpose Coogoon Vallis (Figure 3) and from the western zone by u-section channels which appear to superpose an westwards trending the pattern of sinuous ridges and low-relief channels.

4. Discussion

4.1 The catchment area of Oxia Planum

The catchment represents the source area from which the fluvially transported sedimentary deposits found in Oxia Planum are likely to be derived. The mod-

elled catchment area of 2.1×10^5 km^2 is larger than that of other basins investigated by rovers such as Jezero crater (~0.3×10^5 km^2; Goudge et al., 2015b) or Gale (Ehlmann and Buz, 2015), but similar in scale to the watershed of Hypanis Valles (~4.6×10^5 km^2; Fawdon et al., 2018). To consider the validity of the model catchment we compared the model flow accumulation pathways and watershed boundary to geomorphological observations on orbital images. The low-relief channels and wide flat floored channels match the model flow accumulation pathways across hundreds of kilometres showing that these ancient channels are in good agreement with the current topography (Figure 2).

The ArcHydro-derived flow accumulation network deviates from the network defined by mapping where u-section channels incise older valley landscapes or are deformed by tectonic features. Channels cross into the model catchment from the north, and exit to the west (Figures; 2, 3e, 7 & 10). This suggests the topography must have changed since the formation of the channels. In both instances, tectonic 'wrinkle ridges' deform the pre-existing flow pathways and have created tens to hundreds of meters of relief. In the western region of the model catchment (Figure 6) degraded or inverted impact structures, sinuous ridges and remnant rounded buttes (Figure 6) indicate tens of meters of erosion have altered the topography. This mean the contemporary topography does not represent the paleo-surface into which the channels were eroded and negates the finer-scale validity of model flow accumulation in this area. Given these deviations the paleo catchment probably actually included a larger area to the north but did not include part of the West Quadrant. The west quadrant and the area to the north (just south of Mawrth Vallis) are similar in size, so we consider the model catchment area a reasonable estimate of the contributory area and potential provenance for fluvially transported sediment in Oxia Planum.

4.2 The timing of fluvial activity

Within the model catchment, there is a partially exposed channel network containing three different styles of erosional channels, and a set of sinuous ridges interpreted to be inverted channels or small inverted channel belts. Both the largest wide flat-floored channels, and smallest (low-relief channels) examples of channels, fit within the shape of the present-day regional topography over length scales of hundreds of kilometres but show local deviations from the present day landscape over length scales of tens of kilomteres, where wrinkle ridges modify these channels. In contrast, the intermediate sized u-section channels commonly appear incised into the landscape with well-defined breaks in slope along their banks (e.g. Figure 4). U-section channels superimpose both the floor and banks of wide flat floored channels, as well as occurring along the path of low-relief channels, but the opposite relationship is not observed. This means that u-section style channel formation generally post-dates both the formation of the wide flat floored channels and the initial formation of low-relief channels. The similarities between their flow paths suggests that many u-section channels are reactivations of the low-relief channel flow paths and overprint the medial section

of ancient river profiles now represented only by the wide flat floored channels downstream, and low-relief channels upstream.

The interpretation that the flow paths of the low-relief channels were formed in an ancient landscape is further supported by their along-track transition into sinuous ridge inverted channels. Sinuous ridges are observed in the western portion of the catchment, which has experienced the most erosion (Figure 6). Such topographic inversion of fluvial channels can occur by a variety of processes, including cementation of fluvial sediments to create differential erosion resistance between coarser channel deposits and finer overbank deposits, or later infill of channels and armouring by some subsequent volcanic or impact-sourced materials (e.g.; Pain and Ollier, 1995). All models require later erosion to leave the resistant channel body upstanding in the landscape. Sinuous ridges in the model catchment are not seen to be associated with any volcanic features or impact ejecta, suggesting that the relief inversion has occurred over a wide region in a similar style. This further implies that the differential erosional properties of the channel fill are likely related to endogenic factors (e.g., grain size or cementation) in the channel fill and are an integral part of the ancient landscape (Williams et al., 2009) rather than exogenic factors such as volcaniclastics or impact ejecta. A possible exception is an example of a sinuous ridge trending into a irregular dark depression (Figure 3e).

The implication of these observations for fluvial activity in western Arabia Terra is as follows: firstly, that there was a period of fluvial activity during which Coogoon Valles developed within the ancient topography of the region (Figure 5a). Subsequently, and likely after a hiatus when impact craters accumulated (Quantin-Nataf et al., 2021), a second phase of fluvial erosion led to u-section channel morphologies being superimposed on the pre-existing network (Figure 5c). This later period of incision was likely short-lived because the u-section channels cut into a more mature landscape (Burbank and Anderson, 2009; Howard et al., 2005) but have not reached a sufficient stage of landscape maturity to erase the landscape associated with Coogoon Vallis. Sinuous ridges occur at the same stratigraphic level as low-relief channels so the fluvial activity they represent occurred around the same time as the first stage of development of Coogoon Vallis. To date, no regional stratigraphic markers have been identified that correlate this period to the formation of the many other inverted channels systems observed in Arabia Terra (Davis et al., 2019, 2016), but it would seem improbable that this catchment was not active at a similar time to others in the wider region. We note that many of the inverted channel systems in the Arabia Terra region appear to have been active during the mid- to late-Noachian (Balme et al., 2020; Davis et al., 2019).

These relationships predict that sediment fans associated with u-section channels should postdate the Noachian landscape (which is primarily associated with wide flat floored and low-relief channels). This is validated by observations in the *Oxia Basin* where sediment fans associated with u-section channels superpose both wide flat floored channels and impact craters associated with older surfaces

(Quantin-Nataf et al., 2021). The Stratigraphy also supports a relationship between this initial stage of widespread fluvial activity, associated with the wide flat floored/low-relief channels that developed with the regional relief during the mid/late Noachian, and the regional spectral evidence of hydrated minerology and weathering profiles found in the region (Carter et al., 2015; Loizeau et al., 2007; Michalski and Noe Dobrea, 2007; Noe Dobrea et al., 2010; Poulet et al., 2020). This allows for phyllosilicates in the *Oxia basin* to be either allochtonous or autochtonous depending on rates of alteration and sediment transportation.

4.3 Possible lacustrine activity in craters

Within the modelled catchment area we identified two types of potential paleolake basins associated with impact craters and inter-crater topographic lows. Each of these types (Figures 8, 9, 10) have distinct rim morphologies and show a suite of landforms indicative of lacustrine activity. The landforms we can observe are dependent on the preservation, exposure and context of the lake. Consequently not all possible palaeolakes exhibit every diagnostic landform.

Inlet and outlet channels are the strongest evidence for lake activity, but inlet channels are not common in large crater lakes or rimless crater lakes, despite the evidence from other features that supports a lake intepretation. Inlet channels are seen where craters are located on a topographic rise with a large enough upslope area catchment. Few rimless crater lakes have outlet channels, and only one large crater lake has an outlet channel (Figure 8). This suggests that the formation of outlet channels depends on the physiographic setting of these lakes (i.e. if the groundwater-supplied lake could be episodically supplemented by overland flow; Figure 11). If the large crater lakes and rimless craters with no channels did host lakes at the same time as those in adjacent terrain, then were predominantly supplied by groundwater.

An important case is a chain of four craters (Figure 8c). Here, four interconnected (Figure 8f) large crater lake craters were identified that posses a suite of consilient evidence supporting lacustrine activity (Figure 8d), including a channel breaching a crater rim (Figure 8e). The terrain slopes away from the western end of the channel in all directions (and there is some evidence for a sediment fan) so it is not topographically plausible for this channel to be an inflow channel. This interpretation is supported by the linear elongate streamlined nature of this channel, which we interpret as a single outflow that was not followed by any subsequent persistent or episodic channel erosion. The importance of this feature and these craters is that the water level throughout the crater system must have reached the level of the outlet spillway at least once. A suite of other observations (strand lines, hyperspectral observation of hydrated mineralogy in the layered floor, and a sediment fan) further support the conclusions that these craters host paleolakes.

From this, we interpret that large crater lakes and rimless craters hosted predominantly groundwater-controlled lakes at times when climatic conditions were

conducive to a combination of high groundwater levels and supplementary overland water supply connected to the regional fluvial network. Without detailed study of individual lakes we cannot say when these were active. It is unlikely that lakes in older craters were associated with the earlier phase of fluvial activity; the younger phase of fluvial activity is likely more closely associated with craters hosting well-preserved feature associated with this more intense valley network formation (e.g.; Howard et al., 2005; Irwin III et al., 2005)

4.4 Inter-crater 'lakes'

Irregular Dark Depressions (Figure 10) often overlie or infill channel features, form parts of the floor in other larger crater paleolakes, or are found on plains between craters. On inter-crater plains, Irregular Dark Depressions are often associated with sinuous ridges where the dark material of the irregular dark depressions trends into the inverted channel's topmost resistant layer (Figure 6). This indicates that the infilling or armouring of the channels occurred before the differential erosion that created the sinuous ridges. This erosion has most affected the western part of the catchment, especially in and south of Oxia Planum. Irregular dark depressions have a dark surface which often retains many small craters, indicating that this material type is less susceptible to the processes that erase the smallest part of the crater population (Golombek et al., 2014; Warner et al., 2015) than the surrounding terrains.

Where irregular dark depression like material is identified in Coogoon Vallis and in the north-west of the study area it has been interpreted as tsunami runout deposits (Molina et al., 2017; Rodriguez et al., 2016) that have ponded in topographic lows. Previously, similar surfaces have been attributed to a variety of depoitional processes, including as extrusive volcanic materials due to their commonly observed mafic spectral signatures in Jezero crater (Goudge et al., 2012b) and Oxia Planum (Quantin-Nataf et al., 2021). However, a volcanic interpretation is not necessarily appropriate (e.g.; Edgett, 2005) and in this case is inconsistent with the distribution and variety of contexts seen for Irregular Dark Depressions seen in the *Oxia Basin* catchment: none of the 109 examples within the study area show evidence for volcanic architecture that might be expected from Amazonian volcanism (Brož et al., 2017).

We propose that these dark deposits, when located in crater floors and associated with the channel network, represent allochthonous mafic volcaniclastic/aeolian materials that have been cemented by the last high stand of groundwater. The deposits accumulated in topographic lows associated with the ancient low-relief/wide flat floored channel network, which could have provided hydrological corridors for the groundwater, or mafic enrichment in a desert pavement-like process (Irwin III et al., 2018; Rogers et al., 2018). We do not presume that all deposits exhibiting these properties formed through the same process, or even concurrently, and understanding the context of such deposits is key to understanding their origin; many relief-filling, low albedo deposits occur on Mars.. Furthermore, the process we propose may have occurred at several instances in

time and is probably inconsistently preserved within the study area.

4.5 Implications for Mars's geological history

Our study explores fluvial and lacustrine systems in Western Arabia Terra. From this we have established a sequence of events which constrain the hydrological development of Oxia Planum (Figure 11), spanning events from the mid Noachian to Amazonian in Mars's history.

This sequence began with an early stage of landscape evolution when the main channel of Coogoon Vallis (Figure 3c) was active (Figure 11a). During this time, sediment transported though Paleo-Coogoon Vallis was deposited in an undetermined location to the west of Kilkhampton crater coinciding with the burial of now inverted channels (Figure 6). The rimless craters associated with evidence of lakes (RCL; Figure 9) and the fit low-relief channels into the mature fluvial landscape is comparable to other mid Noachian terrains (e.g.; Irwin et al., 2013).

The implication is that the landscape of the catchment and the formation of Paleo-Coogoon Vallis preserved in the *Oxia Basin* are of at least Mid Noachian age, contemporaneous with best estimates for the age of clay-bearing terrains (Mandon et al., 2021; Parkes-Bowen et al., 2021) at the ExoMars rover landing site (Fawdon et al., 2020; Quantin-Nataf et al., 2021). The scale of Paleo-Coogoon Vallis suggests that sediment was transported and deposited further downslope from the valley we see today, consequently where (and when) Paleo-Coogoon Vallis terminated has three implications for the depositional environment of Oxia Planum.

1. The Paleo-Coogoon terminal deposits are completely Kilkhampton crater. This would suggest that distal deltaic or lacustrine facies infill the *Oxia Basin* if it was a subaqueous basin (either open to Chryse or endorheic) or if the terminal deposits where alluvial fans another process subsequently infilled the Oxia Basin.

2. Paleo-Coogoon terminated in the *Oxia Basin*, west of Kilkhampton crater. In this case deltaic or alluvial facies are infilled the *Oxia basin* in a coastal or lake margin environment.

3. Paleo-Coogoon Vallis terminated terminating further north in Chryse Planitia beyond the Oxia Basin. Then we would expect alluvial or riparian facies in the *Oxia Basin* associated with a regional and an alluvial landscape.

If the deposition was subaqueous then all three of these depositional environments (lacustrine, deltaic, alluvial) can have occurred through different transgressive or regressive periods. Inverted channels in the west of the catchment support an alluvial landscape (Figure 6), but this may only represent what post Noachian denudation (McNeil et al., 2021) has exposed and a grater range of

environments contributing to infilling the *Oxia Basin* are represented in the stratigraphic record.

Following a hiatus (Figure 11b) there was a second phase of fluvial activity (Figure 11c) in which classic 'valley network' style channels were incised into the landscape and sediment fans development at lake high stands. This phase is associated with the peak in valley network formation at the Noachian/Hesperian boundary (Howard et al., 2005; Irwin III et al., 2005) and sediment fan formation around the dichotomy boundary (Di Achille and Hynek, 2010; Fawdon et al., 2018). The modern elevation of Oxia Planum does not match the elevation of other fans, but the presence of tectonic ridges throughout the catchment (e.g; Figures 2, 9, 10; Molina et al., 2017) suggest substantial changes in elevation since their formation. This observation is also supported by models of the development of Tharsis which suggest topographic changes of up to 1km for the region (Chan et al., 2018; Citron et al., 2018; Sholes et al., 2021).

The global influence of Tharsis (Citron et al., 2018) causing long wavelength flexure means that the complex of sediment fan remnants west of Kilkhampton Crater may have been deposited at a substantially different elevation than they are at now. The interspersed episodes of tectonic and fluvial/lacustrine activity suggest that this global scale flexure developed alongside evolving climatic conditions and explains mismatches between the model catchment and geomorphic channel network (Figure 2). Since the Hesperian, further tectonic deformation (Figure 11d) and erosion, especially in the west of the catchment, have altered the landscape and has exhumed older fluvial channel deposits from within surrounding deposits, forming the sinuous ridges seen today (Figure 11e).

This sequence shows that an environment supporting fluvial activity occurred several times, but that later phases were insufficiently intense to totally erase evidence of earlier activity. There was progressively less surface water available over time, but during interfluvial periods sufficient water was still stored globally to permit hydrological activity to recommence.

Figure 11: Sequence of events

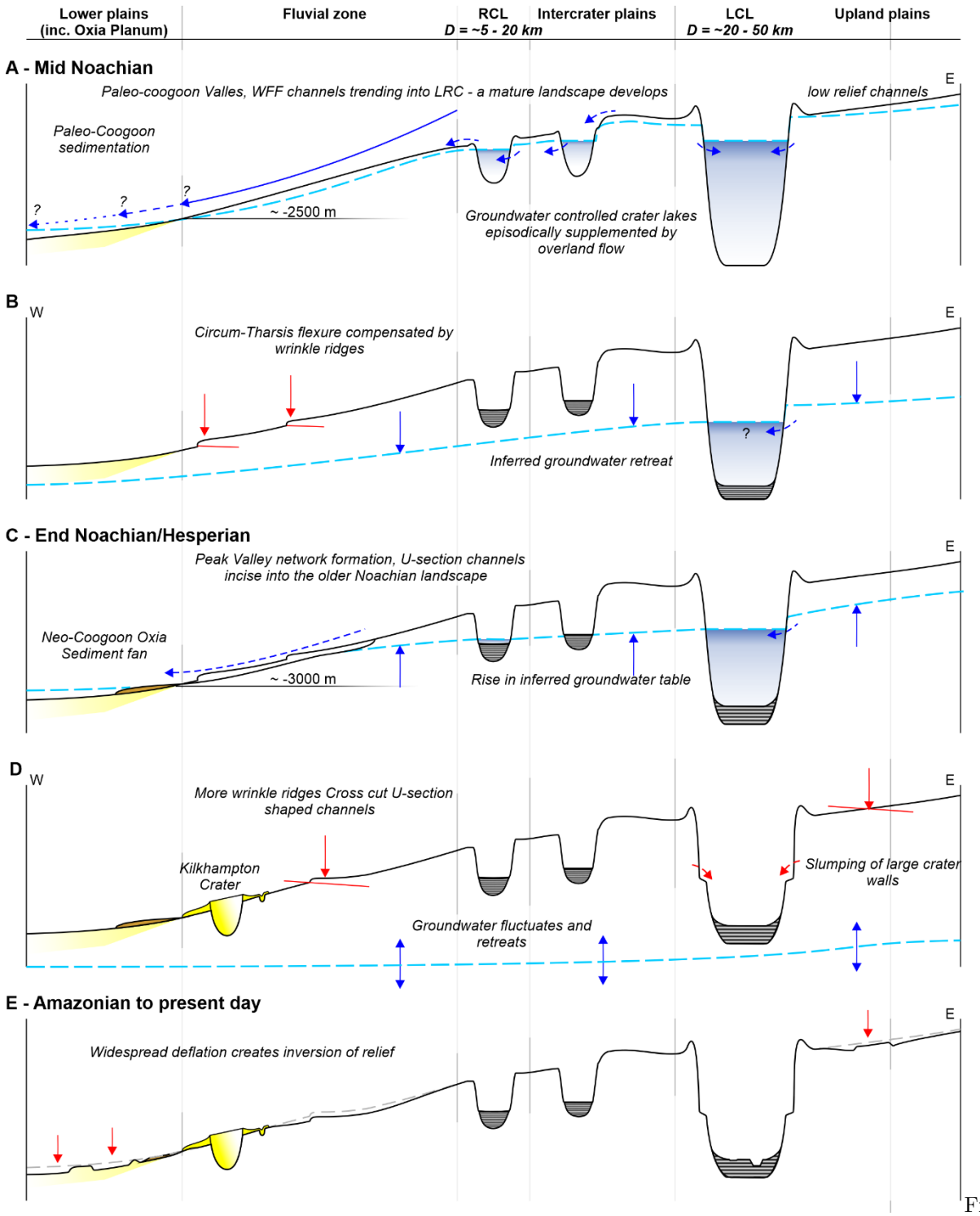
Lower plains
(inc. Oxia Planum)
Fluvial zone
RCL
D = ~5 - 20 km
Intercrater plains
LCL
D = ~20 - 50 km
Upland plains
A - Mid Noachian
Paleo-coogoon Valles, WFF channels trending into LRC - a mature landscape develops
low relief channels
Paleo-Coogoon sedimentation
~ -2500 m
Groundwater controlled crater lakes episodically supplemented by overland flow
B
W
E
Circum-Tharsis flexure compensated by wrinkle ridges
Inferred groundwater retreat
C - End Noachian/Hesperian
Peak Valley network formation, U-section channels incise into the older Noachian landscape
Neo-Coogoon Oxia Sediment fan
~ -3000 m
Rise in inferred groundwater table
D
More wrinkle ridges Cross cut U-section shaped channels
Kilkhampton Crater
Slumping of large crater walls
Groundwater fluctuates and retreats
E - Amazonian to present day
Widespread deflation creates inversion of relief

Figure

11: Schematic showing the relationship between the timing of channel incision, putative lake activity, ground water level, tectonic subsidence and erosion in western Arabia Terra.

5. Conclusions

From our observations of ancient fluvial and lacustrine processes within the hydrological catchment for Oxia Planum, the landing location of the ExoMars 2022 rover, we established a sequence of events for hydrological activity in the catchment (Figure 11) and draw the following conclusions:

- The *Oxia Basin* was fed by an extensive fluvial system with a minimum catchment area of ~2.1×10^5 km^2.
- Within the model catchment we identified three type of fluvial channel (in addition to the main trunk channel of Coogoon Vallis); 'Wide flat floored', 'Narrow U-section' and 'low-relief', and a network of sinuous ridges. We also identified three classes of possible Paleolake deposit; 'large crater lakes', 'rimless crater lakes', and 'irregular dark depressions' which are likely to have been concurrent with the fluvial network.
- We find that there were two major phases of fluvial activity. The first, during the mid Noachian, is associated with the development of the main trunk valley of Coogoon Vallis (Paleo-Coogon Vallis). During this phase the majority of the geomorphic work to form the present day landscape took place. After a hiatus the second phase of activity reactivated relict channels and incised a system of U-section channels (the key sections of which we term Neo-Coogoon Vallis) into the older valley floors.
- We find that large craters with evidence of paleolake deposits are not well integrated into the fluvial system. These craters show evidence for having been sustained by groundwater, and appear to have had contained lakes with multiple different water levels over time.
- Tectonic activity, probably associated with Tharsis formation, occurred after the formation of Paleo-Coogoon Vallis, and again after the reactivation of the fluvial network and formation of the U-section channels. Consequently the contemporary elevation of pour points out of the catchment do not represent the elevation when channels formed.

These conclusions about the development of the ancient environment in the catchment have the following implications for the formation, transportation, and preservation of biomarkers in the *Oxia basin* and for the ExoMars *Rosalind Franklin* Rover mission:

- Sedimentary rock samples obtained by the ExoMars rover are likely to record regionally diverse examples of the Noachian environment, as they might have been transported from anywhere in the extensive catchment.

- Deposits located to the west of Kilkhamption crater, and at the lowest points in the stratigraphy, are likely to be associated with deposition from Paleo-Coogoon Vallis. These could be either deltaic or alluvial sediments, depending on where Paleo-Coogoon Vallis terminated, but a record of this should be preserved within the *Oxia basin* and this determination could be made from rover observations.
- The second phase of activity associated with U-section channel formation was also responsible for the formation of the prominent sediment fan at the eastern margin of the proposed landing site. This phase of fluvial and associated groundwater activity is likely to have imparted a diagenetic overprint on the more ancient clay bearing terrains (Quantin-Nataf et al., 2021).
- The numerous lakes in the catchment appear to have been well-connected into the regional groundwater system. Given that lakes provide excellent potential habitats, biomarkers from these lacustrine systems could have been transported to and concentrated within the *Oxia Basin* during the multiple episodes of regional, linked fluvial and groundwater activity.

Acknowledgements

The data used in this study is freely available from NASA, though the USGS Astrogeology and Arizona State University (CTX; http://themis-data.asu.edu/viewer/ctx#T=0, THEMIS; https://astrogeology.usgs.gov/search/map/Mars/Odyssey/THEMIS-Day-IR-Controlled-Mosaic/Mars-THEMIS-Day-IR-Controlled-Mosaic-Oxia-Palus-00N-315E-100mpp, MOLA; https://astrogeology.usgs.gov/search/map/Mars/GlobalSurveyor/MOLA/Mars_MGS_MOLA_DEM_mosaic
Additionally a database of our observations presented as ESRI shapefiles the MOLA data used to calculate the model catchment and CASSIS image (MY34_006975_165_0) are available though the Open University Open Data Online archive (https://ordo.open.ac.uk/ with Doi: 10.21954/ou.rd.16434606).

The authors gratefully acknowledge the support of the UK Space Agency and the UK Science and Technology Facilities Council (STFC) for supporting science relating to ExoMars Rover landing site section activities and Trace Gas Orbiter participating scientists via the following grants: P. Fawdon, (ST/W002736/1, ST/L00643X/1, ST/R001413/1), M. Balme (ST/R001413/1, ST/L00643X/1), J. Davis (ST/K502388/1, ST/R002355/1 and ST/V002678/1), J. Bridges, (ST/L00643X/1), and S. Gupta (ST/L006413/1) through the ongoing Aroura program. We thank NASA, the CTX camera team, and USGS for the CTX data and maintaining the ISIS and SOCET SET DEM workflows. Additionally we want to thank all the scientist and engineers who have contributed to the ExoMars landing site selection process. The authors wish to thank the CaSSIS spacecraft and instrument engineering teams. CaSSIS is a project

of the University of Bern and funded through the Swiss Space Office via ESA's PRODEX programme. The instrument hardware development was also supported by the Italian Space Agency (ASI) (ASI-INAF agreement no. I/2020-17-HH.0), INAF/Astronomical Observatory of Padova, and the Space Research Center (CBK) in Warsaw. Support from SGF (Budapest), the University of Arizona (Lunar and Planetary Lab.) and NASA are also gratefully acknowledged. Operations support from the UK Space Agency under grant ST/R003025/1 is also acknowledged.

References

Balme, M.R., Gupta, S., Davis, J.M., Fawdon, P., Grindrod, P.M., Bridges, J.C., Sefton-Nash, E., Williams, R.M.E., 2020. Aram Dorsum: An Extensive Mid-Noachian Age Fluvial Depositional System in Arabia Terra, Mars. J. Geophys. Res. Planets 125, e2019JE006244. https://doi.org/10.1029/2019JE006244Bibring, J.-P., Langevin, Y., Mustard, J.F., Poulet, F., Arvidson, R., Gendrin, A., Gondet, B., Mangold, N., Pinet, P., Forget, F., Team, T.O., 2006. Global Mineralogical and Aqueous Mars History Derived from OMEGA/Mars Express Data. Science 312, 400–404. https://doi.org/10.2307/3845879Brož, P., Hauber, E., Wray, J.J., Michael, G., 2017. Amazonian volcanism inside Valles Marineris on Mars. Earth Planet. Sci. Lett. 473, 122–130. https://doi.org/10.1016/j.epsl.2017.06.003Burbank, D.W., Anderson, R.S., 2009. Tectonic geomorphology. John Wiley & Sons.Cabrol, N.A., Grin, E.A., 1999. Distribution, Classification, and Ages of Martian Impact Crater Lakes. Icarus 142, 160–172. https://doi.org/10.1006/icar.1999.6191Cabrol, N.A., Grin, E.A., Carr, M.H., Sutter, B., Moore, J.M., Farmer, J.D., Greeley, R., Kuzmin, R.O., DesMarais, D.J., Kramer, M.G., Newsom, H., Barber, C., Thorsos, I., Tanaka, K.L., Barlow, N.G., Fike, D.A., Urquhart, M.L., Grigsby, B., Grant, F.D., de Goursac, O., 2003. Exploring Gusev Crater with Spirit: Review of science objectives and testable hypotheses. J. Geophys. Res. Planets 108. https://doi.org/10.1029/2002JE002026Carr, M.H., Head, J.W., 2003. Oceans on Mars: An assessment of the observational evidence and possible fate. J. Geophys. Res. Planets 108, n/a-n/a. https://doi.org/10.1029/2002JE001963Carter, J., Loizeau, D., Mangold, N., Poulet, F., Bibring, J.-P., 2015. Widespread surface weathering on early Mars: A case for a warmer and wetter climate. Icarus 248, 373–382. https://doi.org/10.1016/j.icarus.2014.11.011Chan, N.-H., Perron, J.T., Mitrovica, J.X., Gomez, N.A., 2018. New Evidence of an Ancient Martian Ocean From the Global Distribution of Valley Networks. J. Geophys. Res. Planets 123, 2138–2150. https://doi.org/10.1029/2018JE005536Christensen, P., Fergason, R., Edwards, C., Hill, J., 2013. THEMIS-derived thermal inertia mosaic of Mars: Product description and science results. Presented at the Lunar and Planetary Science Conference, p. 2822.Citron, R.I., Manga, M., Hemingway, D.J., 2018. Timing of oceans on Mars from shoreline deformation. Nature 555,

643.Craddock, R.A., Bandeira, L., Howard, A.D., 2018. An Assessment of Regional Variations in Martian Modified Impact Crater Morphology. J. Geophys. Res. Planets 123, 763–779. https://doi.org/10.1002/2017JE005412Craddock, R.A., Maxwell, T.A., 1990. Resurfacing of the Martian Highlands in the Amenthes and Tyrrhena region. J. Geophys. Res. Solid Earth 95, 14265–14278. https://doi.org/10.1029/JB095iB09p14265Davis, J.M., Balme, M., Grindrod, P.M., Williams, R.M.E., Gupta, S., 2016. Extensive Noachian fluvial systems in Arabia Terra: Implications for early Martian climate. Geology 44, 847–850. https://doi.org/10.1130/G38247.1Davis, J.M., Gupta, S., Balme, M.R., Grindrod, P.M., Fawdon, P., Dickeson, Z.I., Williams, R.M.E., 2019. A Diverse Array of Fluvial Depositional Systems in Arabia Terra: Evidence for mid-Noachian to Early Hesperian Rivers on Mars. J. Geophys. Res. Planets 124, 1913–1934. https://doi.org/10.1029/2019JE005976Day, M., Edgett, K.S., Stumbaugh, D., 2019. Ancient Stratigraphy Preserving a Wet-to-Dry, Fluvio-Lacustrine to Aeolian Transition Near Barth Crater, Arabia Terra, Mars. J. Geophys. Res. Planets 124, 3402–3421. https://doi.org/10.1029/2019JE006226Deit, L.L., Hauber, E., Fueten, F., Pondrelli, M., Rossi, A.P., Jaumann, R., 2013. Sequence of infilling events in Gale Crater, Mars: Results from morphology, stratigraphy, and mineralogy. J. Geophys. Res. Planets 118, 2439–2473. https://doi.org/10.1002/2012JE004322Di Achille, G., Hynek, B.M., 2010. Ancient ocean on Mars supported by global distribution of deltas and valleys. Nat. Geosci 3, 459–463.Dickeson, Z.I., Davis, J.M., 2020. Martian oceans. Astron. Geophys. 61, 3.11-3.17. https://doi.org/10.1093/astrogeo/ataa038Edgett, K.S., 2005. The sedimentary rocks of Sinus Meridiani: Five key observations from data acquired by the Mars Global Surveyor and Mars Odyssey orbiters. Int. J. Mars Sci. Explor. 1, 5–58. https://doi.org/10.1555/mars.2005.0002Edgett, K.S., Malin, M.C., 2002. Martian sedimentary rock stratigraphy: Outcrops and interbedded craters of northwest Sinus Meridiani and southwest Arabia Terra. Geophys. Res. Lett. 29, 32–1. https://doi.org/10.1029/2002GL016515Ehlmann, B.L., Buz, J., 2015. Mineralogy and fluvial history of the watersheds of Gale, Knobel, and Sharp craters: A regional context for the Mars Science Laboratory Curiosity's exploration. Geophys. Res. Lett. 42, 264–273. https://doi.org/10.1002/2014GL062553Esri, 2017. How fill works. Fill Works. URL https://desktop.arcgis.com/en/arcmap/10.5/tools/spatial-analyst-toolbox/how-fill-works.htmEsri, 2016. How watershed works. Watershed Works. URL http://pro.arcgis.com/en/pro-app/tool-reference/spatial-analyst/how-watershed-works.htmFassett, C.I., Head III, J.W., 2008. Valley network-fed, open-basin lakes on Mars: Distribution and implications for Noachian surface and subsurface hydrology. Icarus 198, 37–56. https://doi.org/10.1016/j.icarus.2008.06.016Fassett, C.I., Head, J.W., 2011. Sequence and timing of conditions on early Mars. Icarus 211, 1204–1214. https://doi.org/10.1016/j.icarus.2010.11.014Fawdon, P., 2021. Channels and Paleolakes in the Catchment of Oxia Planum. Open Univ. Open Res. Data Online. https://doi.org/10.21954/ou.rd.16434606Fawdon, P., Gupta, S., Davis, J.M., Warner, N.H., Adler, J.B., Balme, M.R., Bell, J.F.,

Grindrod, P.M., Sefton-Nash, E., 2018. The Hypanis Valles delta: The last highstand of a sea on early Mars? Earth Planet. Sci. Lett. 500, 225–241. https://doi.org/10.1016/j.epsl.2018.07.040Fawdon, P., Orgel, C., Grindrod, P., Sefton-Nash, E., Vago, J., Adeli, S., Nass, A., Loizeau, D., Le Deit, L., Thomas, N., Hauber, E., Balme, M., Quantan-Nataf, C., Volat, M., Parks-Bowen, A., Cremonese, G., 2021. A geographic framework for exploring the landing site of the ExoMars 2022 rover at Oxia Planum, Mars. J. Maps.Fawdon, P., Roberts, A.L., Mirino, M.M., 2020. Impact Crater Degradation and The Timing of Resurfacing Events in Oxia Planum, in: Proceedings of the 51th Lunar and Planetary Science Conference. Presented at the 51th Lunar and Planetary Science Conference (2020), Abstract #2240, 51th Lunar and Planetary Science Conference, The Woodlands, Texas, p. #2240.Golombek, M.P., Warner, N.H., Ganti, V., Lamb, M.P., Parker, T.J., Fergason, R.L., Sullivan, R., 2014. Small crater modification on Meridiani Planum and implications for erosion rates and climate change on Mars. J. Geophys. Res. Planets 119, 2522–2547. https://doi.org/10.1002/2014JE004658Goudge, T.A., Aureli, K.L., Head, J.W., Fassett, C.I., Mustard, J.F., 2015a. Classification and analysis of candidate impact crater-hosted closed-basin lakes on Mars. Icarus 260, 346–367. https://doi.org/10.1016/j.icarus.2015.07.026Goudge, T.A., Head, J.W., Mustard, J.F., Fassett, C.I., 2012a. An analysis of open-basin lake deposits on Mars: Evidence for the nature of associated lacustrine deposits and post-lacustrine modification processes. Icarus 219, 211–229. https://doi.org/10.1016/j.icarus.2012.02.027Goudge, T.A., Mustard, J.F., Head, J.W., Fassett, C.I., 2012b. Constraints on the history of open-basin lakes on Mars from the composition and timing of volcanic resurfacing. J. Geophys. Res. Planets 117. https://doi.org/10.1029/2012JE004115Goudge, T.A., Mustard, J.F., Head, J.W., Fassett, C.I., Wiseman, S.M., 2015b. Assessing the mineralogy of the watershed and fan deposits of the Jezero crater paleolake system, Mars. J. Geophys. Res. Planets 120, 775–808. https://doi.org/10.1002/2014JE004782Grant, J.A., 2000. Valley formation in Margaritifer Sinus, Mars, by precipitation-recharged groundwater sapping. Geology 28, 223–226. https://doi.org/10.1130/0091-7613(2000)28<223:VFIMSM>2.0.CO;2Greeley, R., Theilig, E., Guest, J.E., Carr, M.H., Masursky, H., Cutts, J.A., 1977. Geology of Chryse Planitia. J. Geophys. Res. 1896-1977 82, 4093–4109. https://doi.org/10.1029/JS082i028p04093Gwinner, K., Jaumann, R., Hauber, E., Hoffmann, H., Heipke, C., Oberst, J., Neukum, G., Ansan, V., Bostelmann, J., Dumke, A., Elgner, S., Erkeling, G., Fueten, F., Hiesinger, H., Hoekzema, N.M., Kersten, E., Loizeau, D., Matz, K.-D., McGuire, P.C., Mertens, V., Michael, G., Pasewaldt, A., Pinet, P., Preusker, F., Reiss, D., Roatsch, T., Schmidt, R., Scholten, F., Spiegel, M., Stesky, R., Tirsch, D., van Gasselt, S., Walter, S., Wählisch, M., Willner, K., 2016. The High Resolution Stereo Camera (HRSC) of Mars Express and its approach to science analysis and mapping for Mars and its satellites. Planet. Space Sci. 126, 93–138. https://doi.org/10.1016/j.pss.2016.02.014Hauber, E., Brož, P., Jagert, F., Jodłowski, P., Platz, T., 2011. Very recent and wide-spread basaltic volcanism on Mars. Geophys. Res. Lett. 38, n/a-n/a.

https://doi.org/10.1029/2011gl047310Hauber, E., Gwinner, K., Kleinhans, M., Reiss, D., Di Achille, G., Ori, G.-G., Scholten, F., Marinangeli, L., Jaumann, R., Neukum, G., 2009. Sedimentary deposits in Xanthe Terra: Implications for the ancient climate on Mars. Eur. Mars Sci. Explor. Conf. EMSEC 57, 944–957. https://doi.org/10.1016/j.pss.2008.06.009Howard, A.D., Moore, J.M., Irwin III, R.P., 2005. An intense terminal epoch of widespread fluvial activity on early Mars: 1. Valley network incision and associated deposits. J. Geophys. Res. Planets 110. https://doi.org/10.1029/2005JE002459Hynek, B.M., Beach, M., Hoke, M.R.T., 2010. Updated global map of Martian valley networks and implications for climate and hydrologic processes. J. Geophys. Res. Planets 115, n/a-n/a. https://doi.org/10.1029/2009JE003548IAU, 2019. Gazetteer of Planetary Nomenclature: Kilkhampton Crater [WWW Document]. URL https://planetarynames.wr.usgs.gov/Feature/15849?___fsk=-408638816 (accessed 2.22.21).Irwin III, R.P., Howard, A.D., 2002. Drainage basin evolution in Noachian Terra Cimmeria, Mars. J. Geophys. Res. Planets 107, 10–1. https://doi.org/10.1029/2001JE001818Irwin III, R.P., Howard, A.D., Craddock, R.A., Moore, J.M., 2005. An intense terminal epoch of widespread fluvial activity on early Mars: 2. Increased runoff and paleolake development. J. Geophys. Res. Planets 110. https://doi.org/10.1029/2005JE002460Irwin III, R.P., Wray, J.J., Mest, S.C., Maxwell, T.A., 2018. Wind-Eroded Crater Floors and Intercrater Plains, Terra Sabaea, Mars. J. Geophys. Res. Planets 123, 445–467. https://doi.org/10.1002/2017JE005270Irwin, R.P., Tanaka, K.L., Robbins, S.J., 2013. Distribution of Early, Middle, and Late Noachian cratered surfaces in the Martian highlands: Implications for resurfacing events and processes. J. Geophys. Res. Planets 118, 278–291. https://doi.org/10.1002/jgre.20053Ivanov, M.A., Slyuta, E.N., Grishakina, E.A., Dmitrovskii, A.A., 2020. Geomorphological Analysis of ExoMars Candidate Landing Site Oxia Planum. Sol. Syst. Res. 54, 1–14. https://doi.org/10.1134/S0038094620010050Komatsu, G., Brantingham, P.J., Olsen, J.W., Baker, V.R., 2001. Paleoshoreline geomorphology of Böön Tsagaan Nuur, Tsagaan Nuur and Orog Nuur: the Valley of Lakes, Mongolia. Geomorphology 39, 83–98. https://doi.org/10.1016/S0169-555X(00)00095-7Loizeau, D., Mangold, N., Poulet, F., Bibring, J.-P., Gendrin, A., Ansan, V., Gomez, C., Gondet, B., Langevin, Y., Masson, P., Neukum, G., 2007. Phyllosilicates in the Mawrth Vallis region of Mars. J. Geophys. Res. Planets 112. https://doi.org/10.1029/2006JE002877Malin, M.C., Bell, J.F., III, Cantor, B.A., Caplinger, M.A., Calvin, W.M., Clancy, R.T., Edgett, K.S., Edwards, L., Haberle, R.M., James, P.B., Lee, S.W., Ravine, M.A., Thomas, P.C., Wolff, M.J., 2007. Context Camera Investigation on board the Mars Reconnaissance Orbiter. J Geophys Res 112, E05S04. https://doi.org/10.1029/2006je002808Mandon, L., Parkes Bowen, A., Quantin-Nataf, C., Bridges, J.C., Carter, J., Pan, L., Beck, P., Dehouck, E., Volat, M., Thomas, N., Cremonese, G., Tornabene, L.L., Thollot, P., 2021. Morphological and Spectral Diversity of the Clay-Bearing Unit at the ExoMars Landing Site Oxia Planum. Astrobiology 21, 464–480. https://doi.org/10.1089/ast.2020.2292Marzo, G.A., Roush, T.L., Lanza, N.L., McGuire, P.C., Newsom, H.E., Ollila, A.M., Wiseman, S.M., 2009. Association

of phyllosilicates and the inverted channel in Miyamoto crater, Mars. Geophys. Res. Lett. 36. https://doi.org/10.1029/2009GL038703Masursky, H., 1973. An overview of geological results from Mariner 9. J. Geophys. Res. 1896-1977 78, 4009–4030. https://doi.org/10.1029/JB078i020p04009McNeil, J.D., Fawdon, P., Balme, M.R., Coe, A.L., 2021. Morphology, Morphometry and Distribution of Isolated Landforms in Southern Chryse Planitia, Mars. J. Geophys. Res. Planets n/a, e2020JE006775. https://doi.org/10.1029/2020JE006775Michalski, J.R., Noe Dobrea, E.Z., 2007. Evidence for a sedimentary origin of clay minerals in the Mawrth Vallis region, Mars. Geology 35, 951–954.Molina, A., López, I., Prieto-Ballesteros, O., Fernández-Remolar, D., de Pablo, M.Á., Gómez, F., 2017. Coogoon Valles, western Arabia Terra: Hydrological evolution of a complex Martian channel system. Icarus 293, 27–44. https://doi.org/10.1016/j.icarus.2017.04.002Murchie, S., Arvidson, R., Bedini, P., Beisser, K., Bibring, J.P., Bishop, J., Boldt, J., Cavender, P., Choo, T., Clancy, R.T., Darlington, E.H., Des Marais, D., Espiritu, R., Fort, D., Green, R., Guinness, E., Hayes, J., Hash, C., Heffernan, K., Hemmler, J., Heyler, G., Humm, D., Hutcheson, J., Izenberg, N., Lee, R., Lees, J., Lohr, D., Malaret, E., Martin, T., McGovern, J.A., McGuire, P., Morris, R., Mustard, J., Pelkey, S., Rhodes, E., Robinson, M., Roush, T., Schaefer, E., Seagrave, G., Seelos, F., Silverglate, P., Slavney, S., Smith, M., Shyong, W.J., Strohbehn, K., Taylor, H., Thompson, P., Tossman, B., Wirzburger, M., Wolff, M., 2007. Compact Reconnaissance Imaging Spectrometer for Mars (CRISM) on Mars Reconnaissance Orbiter (MRO). J Geophys Res 112, E05S03. https://doi.org/10.1029/2006je002682Neukum, G., Jaumann, R., Hoffmann, H., Hauber, E., Head, J.W., Basilevsky, A.T., Ivanov, B.A., Werner, S.C., van Gasselt, S., Murray, J.B., McCord, T., TeamThe, H.C.-I., 2004. HRSC: the high resolution stereo camera of Mars Express. ESA Spec. Publ. 1240, 1–19.Newsom, H.E., Lanza, N.L., Ollila, A.M., Wiseman, S.M., Roush, T.L., Marzo, G.A., Tornabene, L.L., Okubo, C.H., Osterloo, M.M., Hamilton, V.E., Crumpler, L.S., 2010. Inverted channel deposits on the floor of Miyamoto crater, Mars. MROHiRISE Stud. Mars 205, 64–72. https://doi.org/10.1016/j.icarus.2009.03.030Noe Dobrea, E.Z., Bishop, J.L., McKeown, N.K., Fu, R., Rossi, C.M., Michalski, J.R., Heinlein, C., Hanus, V., Poulet, F., Mustard, R.J.F., Murchie, S., McEwen, A.S., Swayze, G., Bibring, J.-P., Malaret, E., Hash, C., 2010. Mineralogy and stratigraphy of phyllosilicate-bearing and dark mantling units in the greater Mawrth Vallis/west Arabia Terra area: Constraints on geological origin. J. Geophys. Res. Planets 115. https://doi.org/10.1029/2009JE003351Ori, G.G., Marinangeli, L., Baliva, A., 2000. Terraces and Gilbert-type deltas in crater lakes in Ismenius Lacus and Memnonia (Mars). J. Geophys. Res. Planets 105, 17629–17641. https://doi.org/10.1029/1999JE001219Pain, C.F., Ollier, C.D., 1995. Inversion of relief — a component of landscape evolution. Geomorphology 12, 151–165. https://doi.org/10.1016/0169-555X(94)00084-5Palucis, M.C., Dietrich, W.E., Hayes, A.G., Williams, R.M.E., Gupta, S., Mangold, N., Newsom, H., Hardgrove, C., Calef, F., Sumner, D.Y., 2014. The origin and evolution of the Peace Vallis fan system that drains to the Curiosity

landing area, Gale Crater, Mars. J. Geophys. Res. Planets 119, 705–728. https://doi.org/10.1002/2013JE004583Parker, T.J., Gorsline, D.S., Saunders, R.S., Pieri, D.C., Schneeberger, D.M., 1993. Coastal geomorphology of the Martian northern plains. J. Geophys. Res. Planets 98, 11061–11078. https://doi.org/10.1029/93JE00618Parkes-Bowen, A., Bridges, J., Tornabene, L., Mandon, L., Quantin-Nataf, C., Patel, M., Thomas, N., Cremonese, G., 2021. A CaSSIS and HiRISE Map of the Clay-bearing Units at the ExoMars2022 Landing Site in Oxia Planum. Planet. Space Sci. Submitted.Planchon, O., Darboux, F., 2002. A fast, simple and versatile algorithm to fill the depressions of digital elevation models. CATENA 46, 159–176. https://doi.org/10.1016/S0341-8162(01)00164-3Poulet, F., Gross, C., Horgan, B., Loizeau, D., Bishop, J.L., Carter, J., Orgel, C., 2020. Mawrth Vallis, Mars: A Fascinating Place for Future In Situ Exploration. Astrobiology 20, 199–234. https://doi.org/10.1089/ast.2019.2074Quantin-Nataf, C., Carter, J., Mandon, L., Thollot, P., Balme, M., Volat, M., Pan, L., Loizeau, D., Millot, C., Breton, S., Dehouck, E., Fawdon, P., Gupta, S., Davis, J., Grindrod, P.M., Pacifici, A., Bultel, B., Allemand, P., Ody, A., Lozach, L., Broyer, J., 2021. Oxia Planum: The Landing Site for the ExoMars "Rosalind Franklin" Rover Mission: Geological Context and Prelanding Interpretation. Astrobiology 21, 345–366. https://doi.org/10.1089/ast.2019.2191Robbins, S.J., Hynek, B.M., 2012a. A new global database of Mars impact craters 1 km: 1. Database creation, properties, and parameters. J Geophys Res 117, E05004. https://doi.org/10.1029/2011je003966Robbins, S.J., Hynek, B.M., 2012b. A new global database of Mars impact craters 1 km: 2. Global crater properties and regional variations of the simple-to-complex transition diameter. J Geophys Res 117, E06001. https://doi.org/10.1029/2011je003967Rodriguez, J.A.P., Fairén, A.G., Tanaka, K.L., Zarroca, M., Linares, R., Platz, T., Komatsu, G., Miyamoto, H., Kargel, J.S., Yan, J., Gulick, V., Higuchi, K., Baker, V.R., Glines, N., 2016. Tsunami waves extensively resurfaced the shorelines of an early Martian ocean. Sci. Rep. 6, 25106.Rogers, A.D., Warner, N.H., Golombek, M.P., Head III, J.W., Cowart, J.C., 2018. Areally Extensive Surface Bedrock Exposures on Mars: Many Are Clastic Rocks, Not Lavas. Geophys. Res. Lett. 45, 1767–1777. https://doi.org/10.1002/2018GL077030Salese, F., Pondrelli, M., Neeseman, A., Schmidt, G., Ori, G.G., 2019. Geological Evidence of Planet-Wide Groundwater System on Mars. J. Geophys. Res. Planets 124, 374–395. https://doi.org/10.1029/2018JE005802Sholes, S.F., Dickeson, Z.I., Montgomery, D.R., Catling, D.C., 2021. Where are Mars' Hypothesized Ocean Shorelines? Large Lateral and Topographic Offsets Between Different Versions of Paleoshoreline Maps. J. Geophys. Res. Planets 126, e2020JE006486. https://doi.org/10.1029/2020JE006486Smith, D.E., Zuber, M.T., Frey, H.V., Garvin, J.B., Head, J.W., Muhleman, D.O., Pettengill, G.H., Phillips, R.J., Solomon, S.C., Zwally, H.J., Banerdt, W.B., Duxbury, T.C., Golombek, M.P., Lemoine, F.G., Neumann, G.A., Rowlands, D.D., Aharonson, O., Ford, P.G., Ivanov, A.B., Johnson, C.L., McGovern, P.J., Abshire, J.B., Afzal, R.S., Sun, X., 2001. Mars Orbiter Laser Altimeter: Experiment summary after the first year of global mapping of Mars. J Geophys Res 106, 23689–23722.

https://doi.org/10.1029/2000je001364Strahler, A.N., 1957. Quantitative analysis of watershed geomorphology. Eos Trans. Am. Geophys. Union 38, 913–920. https://doi.org/10.1029/TR038i006p00913Tanaka, K.L., 1997. Sedimentary history and mass flow structures of Chryse and Acidalia Planitiae, Mars. J. Geophys. Res. Planets 102, 4131–4149. https://doi.org/10.1029/96JE02862Tanaka, K.L., Skinner, J.A., Dohm, J.M., Irwin, R.P., III, Kolb, E.J., Fortezzo, C.M., Platz, T., Michael, G.G., Hare, T.M., 2014. Geologic map of Mars: U.S. Geological Survey Scientific Investigations Map 3292, scale 1:20,000,000, pamphlet 43 p.Thomas, N., Cremonese, G., Ziethe, R., Gerber, M., Brändli, M., Bruno, G., Erismann, M., Gambicorti, L., Gerber, T., Ghose, K., Gruber, M., Gubler, P., Mischler, H., Jost, J., Piazza, D., Pommerol, A., Rieder, M., Roloff, V., Servonet, A., Trottmann, W., Uthaicharoenpong, T., Zimmermann, C., Vernani, D., Johnson, M., Pelò, E., Weigel, T., Viertl, J., De Roux, N., Lochmatter, P., Sutter, G., Casciello, A., Hausner, T., Ficai Veltroni, I., Da Deppo, V., Orleanski, P., Nowosielski, W., Zawistowski, T., Szalai, S., Sodor, B., Tulyakov, S., Troznai, G., Banaskiewicz, M., Bridges, J.C., Byrne, S., Debei, S., El-Maarry, M.R., Hauber, E., Hansen, C.J., Ivanov, A., Keszthelyi, L., Kirk, R., Kuzmin, R., Mangold, N., Marinangeli, L., Markiewicz, W.J., Massironi, M., McEwen, A.S., Okubo, C., Tornabene, L.L., Wajer, P., Wray, J.J., 2017. The Colour and Stereo Surface Imaging System (CaSSIS) for the ExoMars Trace Gas Orbiter. Space Sci. Rev. 212, 1897–1944. https://doi.org/10.1007/s11214-017-0421-1V. Baker, J. C. Boothroyd, M. H. Carr, J. A. Cutts, P. D. Komar, J. E. Laity, B. K. Lucchitta, M. C. Malin, H. Masursky, D. Nummedal, P. C. Patton, D. Pieri, D. E. Thompson, 1983. Channels and valleys on Mars. GSA Bull. 94, 1035–1054. https://doi.org/10.1130/0016-7606(1983)94<1035:CAVOM>2.0.CO;2Vago, J.L., Spoto, F., Bauer, M., 2018. Oxia Planum favoured for ExoMars surface mission [WWW Document]. Eur. Space Agency. URL https://exploration.esa.int/web/mars/-/60914-oxia-planum-favoured-for-exomars-surface-missionVago, J.L., Westall, F., Pasteur Instrument Teams, L.S.S.W.G., and Other Contributors, Coates, A.J., Jaumann, R., Korablev, O., Ciarletti, V., Mitrofanov, I., Josset, J.-L., De Sanctis, M.C., Bibring, J.-P., Rull, F., Goesmann, F., Steininger, H., Goetz, W., Brinckerhoff, W., Szopa, C., Raulin, F., Westall, F., Edwards, H.G.M., Whyte, L.G., Fairén, A.G., Bibring, J.-P., Bridges, J., Hauber, E., Ori, G.G., Werner, S., Loizeau, D., Kuzmin, R.O., Williams, R.M.E., Flahaut, J., Forget, F., Vago, J.L., Rodionov, D., Korablev, O., Svedhem, H., Sefton-Nash, E., Kminek, G., Lorenzoni, L., Joudrier, L., Mikhailov, V., Zashchirinskiy, A., Alexashkin, S., Calantropio, F., Merlo, A., Poulakis, P., Witasse, O., Bayle, O., Bayón, S., Meierhenrich, U., Carter, J., García-Ruiz, J.M., Baglioni, P., Haldemann, A., Ball, A.J., Debus, A., Lindner, R., Haessig, F., Monteiro, D., Trautner, R., Voland, C., Rebeyre, P., Goulty, D., Didot, F., Durrant, S., Zekri, E., Koschny, D., Toni, A., Visentin, G., Zwick, M., van Winnendael, M., Azkarate, M., Carreau, C., the ExoMars Project Team, 2017. Habitability on Early Mars and the Search for Biosignatures with the ExoMars Rover. Astrobiology 17, 471–510. https://doi.org/10.1089/ast.2016.1533Warner, N.H., Gupta, S., Calef, F., Grindrod, P., Boll, N., Goddard, K., 2015.

Minimum effective area for high resolution crater counting of martian terrains. Icarus 245, 198–240.Wharton, R.A., Crosby, J.M., McKay, C.P., Rice, J.W., 1995. Paleolakes on Mars. J. Paleolimnol. 13, 267–283. https://doi.org/10.1007/BF00682769Williams, R.M.E., Irwin III, R.P., Zimbelman, J.R., 2009. Evaluation of paleohydrologic models for terrestrial inverted channels: Implications for application to martian sinuous ridges. Geomorphology 107, 300–315. https://doi.org/10.1016/j.geomorph.2008.12.015Wray, J.J., Milliken, R.E., Dundas, C.M., Swayze, G.A., Andrews-Hanna, J.C., Baldridge, A.M., Chojnacki, M., Bishop, J.L., Ehlmann, B.L., Murchie, S.L., Clark, R.N., Seelos, F.P., Tornabene, L.L., Squyres, S.W., 2011. Columbus crater and other possible groundwater-fed paleolakes of Terra Sirenum, Mars. J. Geophys. Res. Planets 116. https://doi.org/10.1029/2010JE003694Zuber, M.T., Smith, D.E., Solomon, S.C., Muhleman, D.O., Head, J.W., Garvin, J.B., Abshire, J.B., Bufton, J.L., 1992. The Mars Observer laser altimeter investigation. J. Geophys. Res. Planets 97, 7781–7797. https://doi.org/10.1029/92JE00341